Eidgenössische Technische Hochschule Zürich
Swiss Federal Institute of Technology Zurich

Seminar for Applied Mathematics SAM

Splitting-Based Structure Preserving Discretizations for Magnetohydrodynamics

R. Hiptmair and C. Pagliantini

Research Report No. 2017-18
April 2017

Seminar für Angewandte Mathematik
Eidgenössische Technische Hochschule
CH-8092 Zürich
Switzerland

Funding SNF: 146355

Splitting-Based Structure Preserving Discretizations for Magnetohydrodynamics

Ralf Hiptmair* and Cecilia Pagliantini†

Abstract

We start from the splitting of the equations of single-fluid magnetohydrodynamics (MHD) into a magnetic induction part and a fluid part. We design novel numerical methods for the MHD system based on the coupling of Galerkin schemes for the electromagnetic fields via finite element exterior calculus with finite volume methods for the conservation laws of fluid mechanics. Using a vector potential based formulation, the magnetic induction problem is viewed as an instance of a generalized transient advection problem of differential forms. For the latter, we rely on an Eulerian method of lines with explicit Runge−Kutta timestepping and on structure preserving spatial upwind discretizations of the Lie derivative based on the duality between the contraction of differential forms and the extrusion of chains. The balance laws for the fluid constitute a system of conservation laws with the magnetic induction field as a space and time dependent coefficient, supplied at every time step by the structure preserving discretization of the magnetic induction problem. We describe finite volume schemes based on approximate Riemann solvers adapted to accommodate the electromagnetic contributions to the momentum and energy conservation. A set of benchmark tests for the two-dimensional planar ideal MHD equations provide numerical evidence that the resulting lowest order coupled scheme has excellent conservation properties, is first order accurate for smooth solutions, conservative and stable.

1 Introduction

Plasma phenomena are important in many fields ranging from controlled thermonuclear fusion to astrophysics [25]. The magnetohydrodynamic model provides a mathematical interpretation of the interplay of conducting non-magnetic fluids, like plasmas, with electromagnetic fields. For compressible fluids, the model comprises conservation laws for mass, momentum and energy together with material laws and Maxwell's equations, in the magneto-quasistatic reduction, to describe the evolution of the fields, namely, for spatially homogeneous and isotropic materials,

$$\begin{cases} \partial_t \rho + \operatorname{div}(\rho \mathbf{u}) = 0, & \text{(1.1a)} \\ \partial_t (\rho \mathbf{u}) + \mathbf{div}\left(\rho \mathbf{u} \otimes \mathbf{u} + \left(p + \frac{1}{2}\|\mathbf{B}\|_{\ell^2}^2\right)\mathbb{I} - \mathbf{B} \otimes \mathbf{B}\right) = \mathbf{0}, & \text{(1.1b)} \\ \partial_t E + \operatorname{div}\left(\left(E + p + \frac{1}{2}\|\mathbf{B}\|_{\ell^2}^2\right)\mathbf{u} - (\mathbf{u}\cdot\mathbf{B})\mathbf{B} + \varepsilon\, \mathbf{curl}\mathbf{B} \times \mathbf{B}\right) = 0, & \text{(1.1c)} \\ \partial_t \mathbf{B} + \mathbf{curl}(\mathbf{B} \times \mathbf{u}) + \mathbf{curl}(\varepsilon\, \mathbf{curl}\mathbf{B}) = \mathbf{0}, & \text{(1.1d)} \\ \operatorname{div}\mathbf{B} = 0. & \text{(1.1e)} \end{cases}$$

Here ρ is the fluid density, p the pressure, $\mathbf{u}$ the fluid velocity and $\mathbf{B}$ the magnetic induction field, respectively. The quantity ε is a symmetric positive semi-definite tensor representing the ratio of the electric resistivity and the magnetic permeability. The total energy E is expressed through the equation of state $E = p/(\gamma - 1) + 1/2\rho\|\mathbf{u}\|_{\ell^2}^2 + 1/2\|\mathbf{B}\|_{\ell^2}^2$, where γ is the gas constant.

*Seminar for Applied Mathematics, ETH Zürich, Rämistrasse 101, CH-8092 Zürich, Switzerland.
Email: ralf.hiptmair@sam.math.ethz.ch

†T-5 Applied Mathematics and Plasma Physics Group, Los Alamos National Laboratory, Los Alamos, NM 87545, USA.
Email: pagliantini@lanl.gov, cecilia.pagliantini@sam.math.ethz.ch

In a perfectly conducting plasma, dynamics takes place on time scales faster than the decay of the magnetic field due to Joule or resistive heating and the magnetic field lines are "frozen" into the fluid. Considering the plasma as a perfect conductor corresponds to setting $\varepsilon = 0$ in (1.1) and results in the so-called *ideal* MHD model. Changes of the magnetic field topology during the flow (the reconnection effects) are taken into account in *resistive* MHD models. The relative importance of resistive effects over length scales of order L can be gauged by the magnetic Reynolds number $R_m := \mu_0 \sigma L U$, where U is a characteristic velocity scale of the MHD flow and μ_0 is the permeability of free space. Large values of the Reynolds number correspond to transport times much shorter than the diffusion time for the magnetic fields [25, Section 2.4.1]. The ideal MHD model provides a good approximation of the dynamical phenomena going on in hot and strongly magnetized plasmas. Additionally, robust numerical discretizations of ideal MHD models pave the way to reliable approximations of the resistive MHD problem, even in the presence of locally small magnetic diffusion. For the aforementioned reasons we focus hereafter on the ideal MHD equations as the most challenging case.

The structure of the MHD problem. In three dimensions, the flux Jacobian associated with the MHD equations has eigenvalues [12, Section IV],

$$\begin{aligned}
&\lambda^1 = \mathbf{u}\cdot\mathbf{n} - c_f, \quad \lambda^2 = \mathbf{u}\cdot\mathbf{n} - c_a, \quad \lambda^3 = \mathbf{u}\cdot\mathbf{n} - c_s,\\
&\lambda^4 = \mathbf{u}\cdot\mathbf{n},\\
&\lambda^5 = \mathbf{u}\cdot\mathbf{n} + c_s, \quad \lambda^6 = \mathbf{u}\cdot\mathbf{n} + c_a, \quad \lambda^7 = \mathbf{u}\cdot\mathbf{n} + c_f,
\end{aligned}$$

where $\mathbf{n}$ is the unit normal vector, $a := \sqrt{\gamma p/\rho}$ is the sound speed, $c_a := \sqrt{(\mathbf{B}\cdot\mathbf{n})^2/\rho}$ is the Alfvén speed and the slow and fast magnetoacoustic wave speeds are given by

$$c_s = \frac{1}{\sqrt{2}}\sqrt{a^2 + \frac{\|\mathbf{B}\|_{\ell^2}^2}{\rho} - \sqrt{\left(a^2 + \frac{\|\mathbf{B}\|_{\ell^2}^2}{\rho}\right)^2 - 4a^2\frac{(\mathbf{B}\cdot\mathbf{n})^2}{\rho}}},$$

$$c_f = \frac{1}{\sqrt{2}}\sqrt{a^2 + \frac{\|\mathbf{B}\|_{\ell^2}^2}{\rho} + \sqrt{\left(a^2 + \frac{\|\mathbf{B}\|_{\ell^2}^2}{\rho}\right)^2 - 4a^2\frac{(\mathbf{B}\cdot\mathbf{n})^2}{\rho}}}. \tag{1.2}$$

Hence the MHD equations form a non-strictly hyperbolic system of conservation laws with non-convex flux functions. Since the characteristic fields are not either genuinely nonlinear or linearly degenerate, possible non-regular waves, like compound waves or overcompressive shocks, can develop, in addition to shocks and discontinuities.

Global well-posedness results are not available for nonlinear systems of conservation laws. For genuinely nonlinear one-dimensional systems with Riemann initial data, Lax [44] proved existence and stability of entropy solutions. The generalization to one-dimensional Cauchy problems for initial data with "small" total variation was developed by Glimm [23]. No such results are available for non-convex and non-strictly hyperbolic systems, such as the MHD problem, nor have they been extended to systems of hyperbolic conservation laws in multi-dimensions.

Despite the lack of well-posedness results for the MHD system and the complexity of its wave structure, the relevance of the model in plasma dynamics has spurred the development of numerical methods. On the one hand, numerical simulations of MHD flows can confirm the physical validity of the model and provide insight into the role of the plasma approximation. On the other hand, they can improve the current understanding of plasma behavior in a range of instances, from fusion confinement tests to astrophysical plasma dynamics.

Literature on numerical methods for the MHD equations. The most popular numerical schemes for the MHD problem, and generally for systems of conservation laws, are finite volume methods [24, 45], in which an integral version of the conservation law is solved inside each control volume of the computational domain. Finite volume schemes are rather simple to implement, computationally efficient and well-suited to reproduce the physical manifestations of nonlinear terms. However, a range of complications are related to stability and convergence of fully discrete schemes, to the extension to arbitrarily high order

and unstructured meshes. Other classes of numerical methods have been investigated for the numerical solution of systems of hyperbolic conservation laws, among others, finite element and discontinuous Galerkin methods [15], and spectral methods [26].

In the discretization of the MHD equations, the numerical treatment of the divergence constraint in the context of finite volume and discontinuous Galerkin methods, usually provides control of the error generated by some particular discrete approximation (generally not by others) of the divergence operator of the order of the truncation spatial and temporal error. Nevertheless, near shock discontinuities such error may become very large. Moreover, since the divergence wave is stationary, divergence errors in localized regions can grow in time, and mesh refinement is unable to counteract the numerical pollution of the solution [6]. Violating the divergence constraint at the discrete level might lead to the onset of unphysical plasma transport orthogonal to the magnetic field lines: this causes the loss of conservation of momentum and energy and might trigger numerical instabilities [11]. Within finite volume discretizations, popular methods devised to counteract these drawbacks are the so-called divergence cleaning techniques: the Godunov−Powell method [53], the Generalized Lagrange Multiplier MHD formulation [11, 16], the Constrained Transport method [33, 48, 56], etc. The major disadvantages of such techniques are associated with the expensive computational costs, the need of variable staggering, the difficulties in dealing with arbitrary meshes, the presence of tunable parameters and the introduction of incorrect jump conditions associated with strong shocks [62]. A further issue connected with finite volume discretizations is the design of robust and efficient fully discrete schemes in the presence of the double **curl** operator occurring in the resistive MHD model.

Although finite element methods are more amenable to handling these issues, the fluid dynamics community generally eschews conforming finite element schemes, owing to the difficulties related to the discretization of solutions with low regularity and displaying physical discontinuities. On the other hand, discrete differential forms in the guise of conforming finite elements, the so-called edge elements and generalizations, represent a well-established tool in the numerical discretization of problems in computational electromagnetism [38]. The popularity of numerical schemes based on discrete analogs of differential forms started on the premise that spurious solutions resulting from standard numerical methods often originate from inconsistent discretizations of the physical fields and of the differential operators involved. Formulating numerical approximations *compatible* with the geometric and topological structures underlying the continuum model problem and not just approximating them has paved the way for numerical schemes with superior stability properties and yielding physically consistent solutions. The potential of discrete differential forms has been harnessed, among others, by mimetic finite difference methods [42], discrete exterior calculus [17], and Finite Element Exterior Calculus (FEEC) [4]. FEEC aims at constructing finite element spaces incarnating finite dimensional subcomplexes of certain differential complexes valid at the continuous level (in our case the de Rham complex). By means of commuting projections the discrete fields inherit the topological and algebraic structure of the continuum setting. In the MHD model, this means that a discrete vector potential becomes available and the divergence constraint holds exactly, even for the discrete induction field. At the best of our knowledge, edge and face elements have only been employed in the development of mixed finite element discretizations of incompressible resistive MHD with partial Lie derivative by [57] and more recently in [39]. However, robustness of the aforementioned schemes with respect to large magnetic Reynolds number is still an issue as they rely on standard discretizations of the transport operator.

Scope and outline of the paper. The aim of this work is the design of robust, efficient and stable numerical schemes for the MHD problem based on a splitting strategy which allows to reap the benefits of numerical schemes tailored for different phenomena. Analogously to the splitting strategy advocated in [22], we perform a local (in time) reduction of the MHD system into two systems with discontinuous coefficients: the magnetic induction/potential is advected with a known (discontinuous) velocity field and discretized via finite element exterior calculus, and the **B** field is treated as a discontinuous coefficient in the system of conservation laws for the fluid variables, for which finite volume methods are developed.

The magneto-quasistatic model underlying resistive MHD yields a magnetic advection-diffusion problem for the unknown magnetic induction field. Introducing the magnetic potential, the divergence constraint on the induction field is automatically absorbed into a new advection-diffusion problem, satisfied by the vector potential (*cf.* Appendix A). A generalized advection-diffusion problem for differential forms includes the aforementioned equations and the scalar case as particular instances [35]. In Section 2

we derive and analyze robust numerical methods based on an Eulerian method of lines with explicit timestepping and FEEC-based discretizations via the so-called *extrusion contraction upwind schemes*, first introduced in [34]. In the singular perturbation limit, as in the ideal MHD model, we focus on the generalized pure advection problem.

The balance laws for mass, momentum and energy can be written as a system of conservation laws, named *extended Euler system* [22], with the magnetic induction field as a (discontinuous) varying coefficient obtained as the output of the extrusion contraction upwind scheme. For the numerical treatment of the fluid balance laws we proceed as in [22, Section 2.1], using finite volume schemes with numerical fluxes suitably designed, in Section 3, to accommodate the discontinuous magnetic induction field.

The algorithm obtained by coupling the FEEC-based numerical schemes with the finite volume methods devised for the conservation laws for the fluid is described in Section 4. In Section 5, the FV-FEEC scheme with lowest order spatial discretizations for the two-dimensional planar transient ideal MHD problem on structured meshes is tested on a set of benchmark problems. Conclusions and further research directions are presented in Section 6.

2 Extrusion Contraction Discretization for the Generalized Pure Advection Evolution Problem

The linear eddy current problem underlying the resistive MHD model, in the presence of a conducting fluid moving with velocity $\mathbf{u} = \mathbf{u}(\mathbf{x}, t)$, boils down to the evolution PDE for the vector potential $\mathbf{A}$,

$$\partial_t \mathbf{A} + \mathbf{curl}(\varepsilon \mathbf{curl}\, \mathbf{A}) + \mathbf{curl}\, \mathbf{A} \times \mathbf{u} + \operatorname{grad}(\mathbf{u} \cdot \mathbf{A}) = \mathbf{f}, \tag{2.1}$$

where ε is the magnetic diffusion coefficient; we refer to Appendix A for a detailed derivation of the eddy current model. Problem (2.1) and the well-known scalar advection-diffusion problem belong to a single family of second order evolution problems, the so-called *generalized advection-diffusion* problem. For a unified statement we rely on the language of exterior calculus: for differential k-forms in $\Omega \times I$, with Ω bounded Lipschitz domain in $\mathbb{R}^d$ and $I := [0, T]$, the strong form of the generalized advection-diffusion problem reads

$$\begin{aligned}
\star\partial_t \omega(t) + (-1)^{k+1} \mathsf{d}^{d-k-1} \varepsilon \star \mathsf{d}^k \omega(t) + \star\alpha\omega(t) + \star \mathrm{L}_{\mathbf{u}} \omega(t) &= f(t), && \text{in } \Omega \times I, \\
\operatorname{tr} \omega(t) &= \operatorname{tr} g(t), && \text{on } (\Gamma_{\text{in}} \cup \Gamma_0) \times I, \\
\operatorname{tr}(\mathsf{i}_{\mathbf{n}} \omega(t)) &= \operatorname{tr} s(t), && \text{on } \Gamma_{\text{in}} \times I, \\
\omega(0) &= \omega_0, && \text{in } \Omega,
\end{aligned}$$

where $\omega(t) \in \Lambda^k(\Omega)$ is a time-dependent differential k-form on Ω, $\mathbf{u} : \overline{\Omega} \times I \to \mathbb{R}^d$ is a *given* velocity field, the diffusion coefficient ε and the reaction coefficient α are non-negative and bounded functions $\Omega \to \mathbb{R}$, and the boundary conditions are imposed at the inflow boundary $\Gamma_{\text{in}} := \{\mathbf{x} \in \partial\Omega : \mathbf{u} \cdot \mathbf{n}(\mathbf{x}) < 0\}$, and at $\Gamma_0 := \{\mathbf{x} \in \partial\Omega : \varepsilon > 0\}$. The forcing term and boundary data are $f(t) \in L^2\Lambda^k(\Omega)$, $g(t) \in L^2\Lambda^k(\Gamma_{\text{in}} \cup \Gamma_0)$, and $s(t) \in L^2\Lambda^{k-1}(\Gamma_{\text{in}})$. Moreover, with the standard notation of exterior calculus, see e.g. [36, Section 1.1], $\star$ is the Hodge operator, d^k is the exterior derivative, $\mathsf{i}_{\mathbf{n}}$ is the contraction by the vector $\mathbf{n}$ normal to the boundary, and $\mathrm{L}_{\mathbf{u}}$ is the Lie derivative.

It is well known that for the scalar advection-diffusion equation standard Galerkin discretizations with Lagrangian finite elements break down in the singular perturbation limit of vanishing diffusion. The onset of spurious oscillations reflects the weakly coercive nature of the problem in the energy norm. A plethora of stabilization mechanisms have been devised to counteract the spreading of unphysical oscillations while avoiding an excessive smearing of the solution [55]: residual-based methods such as SUPG (streamline upwind Petrov Galerkin) [40] or the Galerkin least squares [41], discontinuous Galerkin approximations with *upwind* numerical fluxes at element interfaces, see [3] and references therein, etc.

In this work, we explore a class of extrusion contraction upwind schemes, namely finite element conforming discretizations of the transport operator, the Lie derivative, built on the duality between the contraction operator and the extrusion of manifolds. As we shall see in the forthcoming presentation, these

methods incorporate an upwinding element and deliver numerical schemes with favorable stability and structure preserving properties. The terminology extrusion contraction upwind schemes was introduced in [34] where, taking the cue from the monotone upwind quadrature scheme of Tabata [60], the authors proposed an upwind discretization of the Lie derivative in the advection-diffusion problem exploiting the duality between contraction and extrusion suggested in [9]. While the focus of the work [34] is on the stationary scalar advection-diffusion problem, emphasis on the transient pure advection problem for 1-forms is placed in the discretization scheme suggested in [50]. The approach of the latter work resembles more a finite volume technique: the contraction of a discrete $(k+1)$-form is approximated by projecting the extrusion of every mesh k-cell onto the mesh aligned $(k+1)$-dimensional subspaces, and then summing the contributions of $(k+1)$-dimensional finite volume discretizations applied to each of the projections. In a FEEC perspective, we adopt a strategy analogous to [34].

With the ideal MHD problem in mind, we focus on the transient generalized pure advection problem: numerical schemes proving robust in this case are also suitable for the generalized problem when augmented with a standard $H\Lambda^k(\Omega)$-conforming Galerkin discretization of the non-vanishing diffusion term. The generalized pure advection initial boundary value problem in the space-time domain $\Omega \times I$, in weak formulation reads: For $f \in C^0(I; L^2\Lambda^k(\Omega))$ and $\omega_0 \in W_{|t=0}$, find $\omega \in C^1(I; L^2\,\Lambda^k(\Omega)) \cap C^0(I; W)$ such that

$$\begin{aligned} (\partial_t \omega, \eta)_\Omega + (\alpha\omega, \eta)_\Omega + (\mathrm{L}_{\mathbf{u}}\omega, \eta)_\Omega &= (f, \eta)_\Omega, \\ (\omega(0), \eta)_\Omega &= (\omega_0, \eta)_\Omega, \end{aligned} \tag{2.2}$$

for all $\eta \in L^2\,\Lambda^k(\Omega)$, where $(\cdot,\cdot)_\Omega$ denotes the $L^2\,\Lambda^k(\Omega)$ inner product $(\omega,\eta)_\Omega := \int_\Omega \omega \wedge \star\eta$, and the variational spaces V and W are defined as

$$\begin{aligned} V &:= \{\omega \in L^2\Lambda^k(\Omega) :\ \mathrm{L}_{\mathbf{u}}\omega \in L^2\Lambda^k(\Omega)\,,\ \int_{\Gamma_{\mathrm{in}}} \mathrm{tr}\,\mathsf{i}_{-\mathbf{u}}(\omega \wedge \star\omega) < \infty\}, \\ W_{|t} &:= \{\omega \in V :\ \mathrm{tr}\,\omega = g,\ \mathrm{tr}\,\mathsf{i}_{\mathbf{n}}\omega = s \text{ on } \Gamma_{\mathrm{in}},\ g(t) \in L^2\Lambda^k(\Gamma_{\mathrm{in}}),\ s(t) \in L^2\Lambda^{k-1}(\Gamma_{\mathrm{in}})\}. \end{aligned}$$

For velocity fields uniformly continuous in time and Lipschitz continuous in space, $\mathbf{u} \in C^0(I; W^{1,\infty}(\Omega))$, the following "coercivity" condition on the velocity: there exists a constant $\alpha_0 > 0$ such that

$$\int_\Omega \big(\alpha + \frac{1}{2}(\mathrm{L}_{\mathbf{u}(\cdot,t)} + \mathcal{L}_{\mathbf{u}(\cdot,t)})\big)\omega \wedge \star\omega \geq \alpha_0 \int_\Omega \omega \wedge \star\omega, \qquad \forall\, \omega \in L^2\Lambda^k(\Omega)\,,\ \forall\, t \in I, \tag{2.3}$$

with $\mathcal{L}_{\mathbf{u}} = -(-1)^{k(d-k)} \star \mathrm{L}_{\mathbf{u}} \star$, ensures that the variational problem (2.2) is well-posed. Expressions in vector proxies of the "coercivity" condition (2.3) on the velocity field can be found in [52, Table 3.1]. However, MHD solutions feature shocks that give rise to *discontinuous velocities*. A well-posedness theory for velocity fields with less regularity is available only for scalar advection. We refer to [36, Section 1.2] for a more detailed discussion on the well-posedness of the generalized advection problem.

Following a method of lines strategy, a suitable spatial discretization of the time-independent advection operator can be coupled with an explicit Runge−Kutta scheme. Therefore, we first consider the stationary generalized advection boundary value problem for a k-form $\omega \in \Lambda^k(\Omega)$: Find $\omega \in V$ such that

$$\begin{aligned} \alpha\omega + \mathrm{L}_{\mathbf{u}}\omega &= f, \quad \text{in } \Omega, \\ \mathrm{tr}\,\omega &= g, \quad \text{on } \Gamma_{\mathrm{in}}, \\ \mathrm{tr}\,\mathsf{i}_{\mathbf{n}}\omega &= s, \quad \text{on } \Gamma_{\mathrm{in}}, \end{aligned} \tag{2.4}$$

with $f \in L^2\,\Lambda^k(\Omega)$, $g \in L^2\Lambda^k(\Gamma_{\mathrm{in}})$, $s \in L^2\Lambda^{k-1}(\Gamma_{\mathrm{in}})$. As anticipated, we aim at finding a stable numerical discretization of the advection operator, the Lie derivative $\mathrm{L}_{\mathbf{u}}$, based on polynomial $H\Lambda^k(\Omega)$-conforming discrete differential forms. With the Cartan's formula in mind $\mathrm{L}_{\mathbf{u}} = \mathsf{d}^{k-1}\mathsf{i}_{\mathbf{u}} + \mathsf{i}_{\mathbf{u}}\mathsf{d}^k$, this boils down to finding discrete counterparts of the exterior derivative d^k and of the contraction operator $\mathsf{i}_{\mathbf{u}}$.

In the following, let $\{\mathcal{T}_h\}_{h>0}$ be a family of cellular decompositions of the domain Ω such that every $\mathcal{T}_h$ is either a finite element simplicial mesh in the sense of Ciarlet [14, Section 3.1], or it is a tensor product mesh. Furthermore, let $\Lambda_h^k(\mathcal{T}_h)$, $0 \leq k \leq d$, be an $H\Lambda^k(\Omega)$-conforming space of polynomial discrete differential forms, see e.g. [52, Section 2.4.1]. Let $\Lambda_{h,r}^k(\mathcal{T}_h)$, $0 \leq k \leq d$, be the $H\Lambda^k(\Omega)$-conforming space of piecewise polynomial discrete differential k-forms of degree at most $r \geq 1$, namely

$$\Lambda_{h,r}^k(\mathcal{T}_h) := \{\omega_h \in H\Lambda^k(\Omega) :\ \omega_{h|_T} \in \zeta_r^k(T),\ T \in \mathcal{T}_h\}, \tag{2.5}$$

where the local shape functions are $\zeta_r^k(T) = \mathcal{P}_r\Lambda^k(T)$ or $\zeta_r^k(T) = \mathcal{P}_r^-\Lambda^k(T)$ on simplicial meshes [37, 4], and $\zeta_r^k(T) = \mathcal{Q}_r^-\Lambda^k(T)$ [2] or $\zeta_r^k(T) = \mathcal{S}_r\Lambda^k(T)$ [1] on Cartesian meshes.

Let $0 \le k \le n$ and $r \ge 1$. On a d-cell $T \in \mathcal{T}_h$, the degrees of freedom of $\zeta_r^k(T)$ are defined on every j-cell $f_j \in \Delta_j(T)$, with $k \le j \le M_{\min}^{r,k}$, as

$$\omega \in \zeta_r^k(T) \longmapsto W_{f_j,T}^\ell(\omega) := \int_{f_j} \operatorname{tr}\omega \wedge \eta_j^\ell \qquad \forall \ell = 1, \dots, N_j, \tag{2.6}$$

where $\{\eta_j^\ell\}_{\ell=1}^{N_j}$ is a basis of $\overline{\zeta}_{r,j}^k(T)$ defined as $\overline{\zeta}_{r,j}^k(T) = \mathcal{P}_{r-j+k}^-\Lambda^{j-k}(f_j)$ if $\zeta_r^k(T) = \mathcal{P}_r\Lambda^k(T)$, $\overline{\zeta}_{r,j}^k(T) = \mathcal{P}_{r-j+k-1}\Lambda^{j-k}(f_j)$ if $\zeta_r^k(T) = \mathcal{P}_r^-\Lambda^k(T)$, $\overline{\zeta}_{r,j}^k(T) = \mathcal{P}_{r-2(j-k)}\Lambda^{j-k}(f_j)$ if $\zeta_r^k(T) = \mathcal{S}_r\Lambda^k(T)$, and $\overline{\zeta}_{r,j}^k(T) = \mathcal{Q}_{r-1}^-\Lambda^{j-k}(f_j)$ if $\zeta_r^k(T) = \mathcal{Q}_r^-\Lambda^k(T)$. The number of degrees of freedom associated with the mesh faces is

$$M_{\min}^{r,k} := \begin{cases} \min\{d, \lfloor r/2 \rfloor + k\} & \text{if } \Lambda_{h,r}^k(\mathcal{T}_h) = \mathcal{S}_r\Lambda^k(\mathcal{T}_h), \\ \min\{d, r+k-1\} & \text{otherwise.} \end{cases} \tag{2.7}$$

Local projection operators onto polynomial spaces of differential forms can be defined as $\mathcal{I}_{r,T}^k : \Lambda^k(T) \to \zeta_r^k(T)$, $T \in \mathcal{T}_h$,

$$W_{f_j,T}^\ell(\mathcal{I}_{r,T}^k\omega) := \int_{f_j} \operatorname{tr}(\mathcal{I}_{r,T}^k\omega) \wedge \eta = \int_{f_j} \operatorname{tr}\omega \wedge \eta, \qquad \forall\, \eta \in \overline{\zeta}_{r,j}^k(T), \quad f_j \in \Delta_j(T), \quad k \le j \le M_{\min}^{r,k}.$$

2.1 Contraction and Extrusion

The Lie derivative is a coordinate-independent operator which measures the rate of change of a differential form along the flow of a vector field. It is the generalization to k-forms of the spatial part of the material derivative which represents differentiation along the characteristic curves, and hence measures the rate of change observed by a material particle moving with a fluid. Let $\mathcal{M}_d$ be a d-dimensional smooth manifold and let $\mathbf{u}$ be a smooth vector field on $\mathcal{M}_d$. By introducing the *flow* of the vector field $\mathbf{u}$ on the manifold $\mathcal{M}_d$, namely $\Phi : \mathbb{R} \times \mathcal{M}_d \to \mathcal{M}_d$ such that $\partial_t\Phi(t,x) = \mathbf{u}(\Phi(t,x),t)$ with $\Phi(0,x) = x$, the Lie derivative of a differential k-form $\omega \in \Lambda^k(\Omega)$ is

$$\mathrm{L}_{\mathbf{u}}\omega = \left.\frac{d}{dt}\right|_{t=0} \Phi_t^*\omega.$$

The orbits of smooth manifolds under the flow define the so-called extrusion (see Figure 1).

Definition 2.1 (Extrusion)**.** Let $\mathcal{M}_d$ be an d-dimensional smooth oriented manifold. Let $\mathcal{S}_j$ be a j-dimensional submanifold of $\mathcal{M}_d$, the extrusion $\mathsf{Ext}_{\mathbf{u}}(\mathcal{S}_j,t)$ of $\mathcal{S}_j$ by the smooth vector field $\mathbf{u}$, at time t, is the $(j+1)$-dimensional manifold formed by the union of the submanifolds obtained by sweeping $\mathcal{S}_j = \Phi(0,\mathcal{S}_j)$ along the flow of $\mathbf{u}$ to the submanifold $\Phi(t,\mathcal{S}_j)$. Specifically, $\mathsf{Ext}_{\mathbf{u}}(\mathcal{S}_j,t) = \bigcup_{s\in[0,t]} \Phi(s,\mathcal{S}_j)$ with orientation given by $\partial\mathsf{Ext}_{\mathbf{u}}(\mathcal{S}_j,t) = \Phi(t,\mathcal{S}_j) - \Phi(0,\mathcal{S}_j) - \mathsf{Ext}_{\mathbf{u}}(\partial\mathcal{S}_j,t)$.

The contraction of alternating $(k+1)$-forms by a smooth vector field $\mathbf{u}$ is defined as the k-form such that $(\mathsf{i}_{\mathbf{u}}\omega)(\mathbf{x})(v_1,\dots,v_k) = \omega(\mathbf{x})(\mathbf{u}(\mathbf{x}),v_1,\dots,v_k)$, for $\omega \in \operatorname{Alt}^{k+1}V$ and $(v_1,\dots,v_k) \in V^k$, V being a real vector space and $\operatorname{Alt}^{k+1}V$ the space of alternating algebraic $(k+1)$-forms on V. Pointwise application of the foregoing construction yields a definition of the contraction operator on smooth differential forms. The correspondences between the contraction of differential forms and proxy fields is recalled in Table 1. Alternatively, with the concept of extrusion, the contraction $\mathsf{i}_{\mathbf{u}}\omega \in \Lambda^k(\mathcal{M}_d)$ of a smooth $(k+1)$-form $\omega \in \Lambda^{k+1}(\mathcal{M}_d)$ on a k-dimensional smooth oriented submanifold $\mathcal{M}_k$ can be defined as the instantaneous change of ω evaluated on the extrusion of $\mathcal{M}_k$ [9, Equation (14)], namely

$$\langle \mathsf{i}_{\mathbf{u}}\omega, \mathcal{M}_k\rangle = \lim_{t\searrow 0} \frac{1}{t}\langle \omega, \mathsf{Ext}_{\mathbf{u}}(\mathcal{M}_k,t)\rangle, \tag{2.8}$$

where $\langle\cdot,\cdot\rangle$ denotes the chain-cochain duality pairing.

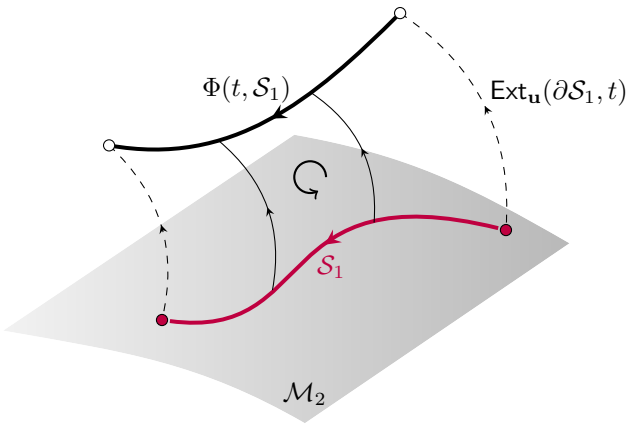

Figure 1: Sketch of the extrusion of an oriented path $\mathcal{S}_1$.

$\omega \in \Lambda k$	$k=0$	$k=1$	$k=2$	$k=3$
$\mathsf{i}_{\mathbf{u}}\omega$	$-$	$\mathbf{u}\cdot\mathbf{w}$	$\mathbf{w}\times\mathbf{u}$	$w\mathbf{u}$

Table 1: Contraction of differential forms: exterior calculus notations and corresponding expressions for vector proxies $\mathbf{w}$, w in $\mathbb{R}^3$.

2.2 Upwind Discrete Contraction via Extrusion

In view of Stokes's theorem [58, Theorem 1.2.7], a discrete definition of exterior derivative is directly given through the coboundary operator ∂, i.e., $\langle \mathsf{d}^k\omega_h, c_{k+1}\rangle = \langle \omega_h, \partial c_{k+1}\rangle$ for all $\omega_h \in \Lambda_h^k(\mathcal{T}_h)$ where ∂c_{k+1} is a k-chain, boundary of the $(k+1)$-chain c_{k+1}. However, the lack of smoothness of discrete differential forms does not allow to define analogously a discrete contraction operator as the restriction to discrete spaces. Since in a finite element discretization approach the aim is to find suitable approximations of integrals of forms, the concept of extrusion of a manifold by the flow of a vector field offers a natural way to define the integral of a contracted discrete differential form over such manifold. A discrete contraction and its combination with the coboundary operator pave the way to discretizations of the Lie derivative.

In greater detail, the duality formula (2.8) expresses the fact that the contraction of a smooth $(k+1)$-form over a k-dimensional manifold is equal to the instantaneous change of the form over the extrusion of the manifold. Equivalently, (2.8) can be rewritten in an "upwind" fashion, if the k-dimensional submanifold $\mathcal{M}_k$ is extruded *backward in time*, namely

$$\langle \mathsf{i}_{\mathbf{u}}\omega, \mathcal{M}_k\rangle = -\lim_{t\searrow 0}\frac{1}{t}\langle \omega, \mathsf{Ext}_{\mathbf{u}}(\mathcal{M}_k, -t)\rangle, \qquad \forall\, \omega \in \Lambda^{k+1}(\mathcal{M}_d). \tag{2.9}$$

The lack of smoothness of discrete differential forms $\omega_h \in \Lambda_h^{k+1}(\mathcal{T}_h)$ implies that

$$\langle \mathsf{i}_{\mathbf{u}}\omega_h, c_k\rangle = \lim_{t\searrow 0}\frac{1}{t}\int_{\mathsf{Ext}_{\mathbf{u}}(c_k,t)}\omega_h \neq -\lim_{t\searrow 0}\frac{1}{t}\int_{\mathsf{Ext}_{-\mathbf{u}}(c_k,t)}\omega_h = \langle -\mathsf{i}_{-\mathbf{u}}\omega_h, c_k\rangle, \tag{2.10}$$

where $c_k \in \Delta_k(\mathcal{T}_h)$ and $\Delta_k(\mathcal{T}_h)$ denotes the set of all k-faces, $0 \le k \le d$, of $\mathcal{T}_h$. Finding a discretization of the contraction operator requires therefore to associate suitable degrees of freedom to the discrete $(k-1)$-form $\mathsf{i}_{\mathbf{u}}\omega_h$, [34, Section 1.2]. This is achieved via the duality between the contraction of a differential form by a vector field and the extrusion of a manifold, by imposing in the discrete setting the equality (2.10) valid at the continuous level: every k-cell of $\mathcal{T}_h$ is extruded backward in time and then the discrete form is evaluated over the extruded $(k+1)$-manifold. Moreover, instead of approximating the "values" of the contraction $\mathsf{i}_{\mathbf{u}}\omega_h$ at the k-cells, one can look for an approximation of their extrusion, rephrasing the problem into how to represent the extrusion of a k-dimensional manifold as a combination of $(k+1)$-chains. The extrusion of 0-chains can be tackled as follows.

Example 2.2. The case of 1-manifolds on a two-dimensional mesh $\mathcal{T}_h$ can be analyzed as in [9, Section III]: an oriented line $\overline{\mathbf{z}-\mathbf{y}}$ in a fixed n-cell $T \in \mathcal{T}_h$ can be described by a weighted sum of edges as,

$$\overline{\mathbf{z}-\mathbf{y}} \text{ “}=\text{”} \sum_{e\in\Delta_1(\mathcal{T}_h)\cap\partial T} \langle \psi_e, \overline{\mathbf{z}-\mathbf{y}}\rangle \overline{e},$$

where ψ_e is the Whitney form associated with the oriented edge $e = \{\mathbf{z}_1, \mathbf{z}_2\}$, with vector proxy $\psi_e = \lambda_{\mathbf{z}_1}\mathrm{grad}\lambda_{\mathbf{z}_2} - \lambda_{\mathbf{z}_2}\mathrm{grad}\lambda_{\mathbf{z}_1}$, and $\lambda_{\mathbf{z}_i}$ being the barycentric coordinate at the node $\mathbf{z}_i$, $i \in \{1, 2\}$. Let $\mathbf{z} \in \Delta_0(\mathcal{T}_h)$ be a 0-cell of $\mathcal{T}_h$ and let us assume that the path $\overline{\mathbf{z}-\mathbf{y}} := -\lim_{t\searrow 0} \mathsf{Ext}_{-\mathbf{u}}(\mathbf{z}, t)/t$ is contained in an n-cell $T^{\mathsf{upw}}_{\mathbf{z}} \in \mathcal{T}_h$. Given a discrete 1-form $\omega_h \in \Lambda^1_h(\mathcal{T}_h)$ we can define the degree of freedom of its contraction at $\mathbf{z} \in \Delta_0(T)$ by enforcing $\langle \mathsf{i}_{\mathbf{u}}\omega_h, \mathbf{z}\rangle = -\lim_{t\searrow 0}\langle \omega_h, \mathsf{Ext}_{-\mathbf{u}}(\mathbf{z}, t)\rangle/t$. In this way,

$$\begin{aligned}\langle \mathsf{i}_{\mathbf{u}(\mathbf{x})}\omega_h(\mathbf{x}), \mathbf{z}\rangle = \langle \omega_h(\mathbf{x}), \overline{\mathbf{z}-\mathbf{y}}\rangle &= \sum_{e\in\Delta_1(\mathcal{T}_h)\cap\partial T^{\mathsf{upw}}_{\mathbf{z}}} \langle \psi_e(\mathbf{x}), \overline{\mathbf{z}-\mathbf{y}}\rangle\langle \omega_h(\mathbf{x}), \overline{e}\rangle \\ &= \langle \omega_h(\mathbf{x})_{|_{T^{\mathsf{upw}}_{\mathbf{z}}}}, \overline{\mathbf{z}-\mathbf{y}}\rangle = \langle \mathsf{i}_{\mathbf{u}(\mathbf{x})}\omega_{h|_{T^{\mathsf{upw}}_{\mathbf{z}}}}(\mathbf{x}), \mathbf{z}\rangle.\end{aligned}$$

Once the degrees of freedom of the contraction of a discrete form at the mesh cells are uniquely defined, a global contraction operator can be introduced through a (global) reconstruction, by interpolating the contraction of a discrete k-form into some space of $H\Lambda^{k-1}(\Omega)$-conforming discrete differential forms. Since we are interested in piecewise polynomial discretizations, we consider interpolation spaces of $H\Lambda^k(\Omega)$-conforming polynomial discrete differential forms $\Lambda^k_{h,p}(\mathcal{T}_h)$ of type (2.5), for some polynomial degree $p \geq 1$ which might differ from the polynomial degree of the approximation spaces.

As a preliminary step, in order to introduce an interpolation operator of contraction, we need to identify an ‘‘upwind direction’’ at the mesh faces. The d-cell $T^{\mathsf{upw}}_{f_j} \in \mathcal{T}_h$ is said to lie in the upwind direction of $f_j \in \Delta_j(\mathcal{T}_h)$ determined by the vector field $\mathbf{u}$ if the extrusion $\mathsf{Ext}_{-\mathbf{u}}(f_j, t)$ is contained in $T^{\mathsf{upw}}_{f_j}$, for t small enough. We make the assumption that $T^{\mathsf{upw}}_{f_d} = T$ and that $T^{\mathsf{upw}}_{f_0} = T$ for all $f_0 \in \Delta_0(T) \setminus \partial T$.

Definition 2.3 (Upwind interpolation of contraction)**.** Let $\mathcal{T}_h$ be a cellular complex on $\Omega \subset \mathbb{R}^d$. Let $\omega_h \in \Lambda^{k+1}_h(\mathcal{T}_h)$, $0 \leq k \leq d-1$, be a discrete differential $(k+1)$-form and let $\mathbf{u}$ be a smooth vector field. Given a polynomial space of differential forms $\Lambda^k_{h,p}(\mathcal{T}_h) \subset H\Lambda^k(\Omega)$, $p \geq 1$, as in (2.5), the upwind interpolation operator $\mathcal{I}^k_{\mathbf{u},p} : L^2\Lambda^k(\Omega) \to \Lambda^k_{h,p}(\mathcal{T}_h)$ is defined as,

$$\mathcal{I}^k_{\mathbf{u},p}(\mathsf{i}_{\mathbf{u}}\omega_h) = \sum_{j=k}^{M^{p,k}_{\min}} \sum_{f_j\in\Delta_j(\mathcal{T}_h)} \sum_{\ell=1}^{N_j} W^\ell_{f_j}(\mathsf{i}_{\mathbf{u}}\omega_{h|_{T^{\mathsf{upw}}_{f_j}}})\psi^\ell_j,$$

where $T^{\mathsf{upw}}_{f_j} \in \mathcal{T}_h$ is the d-cell lying in the upwind direction of f_j, determined by the vector field $\mathbf{u}$. Here, $\{W^\ell_{f_j}\}_{j,\ell} \subset \mathbb{R}$ are the degrees of freedom (2.6) associated with the j-dimensional mesh cells, $\{\psi^\ell_j\}_{j,\ell}$ is a basis of $\Lambda^k_{h,p}(\mathcal{T}_h)$, and $M^{p,k}_{\min}$ is the number of degrees of freedom (2.7) associated with the mesh faces.

Note that, $\mathcal{I}^k_{\mathbf{u},p}(\mathsf{i}_{\mathbf{u}}\omega_h) = \mathsf{i}_{\mathbf{u}}\omega_h$ for every $\mathsf{i}_{\mathbf{u}}\omega_h \in \Lambda^k_{h,p}(\mathcal{T}_h) \subset H\Lambda^k(\Omega)$. Moreover, the degrees of freedom interior to the mesh elements are not affected by upwinding.

2.3 Discrete Lie derivative

Using the discretization of the contraction operator according to Definition 2.3, the *discrete* Lie derivative is defined as,

$$\begin{aligned}\mathrm{L}^h_{\mathbf{u}} : \Lambda^k_{h,r}(\mathcal{T}_h) &\longrightarrow \Lambda^k_{h,p}(\mathcal{T}_h) \\ \omega_h &\longmapsto \mathcal{I}^k_{\mathbf{u},p}(\mathsf{i}_{\mathbf{u}}\mathsf{d}^k\omega_h) + \mathsf{d}^{k-1}\mathcal{I}^{k-1}_{\mathbf{u},p^-}(\mathsf{i}_{\mathbf{u}}\omega_h),\end{aligned} \tag{2.11}$$

where $p^- \geq 1$ is such that $\mathsf{d}^{k-1}\Lambda^{k-1}_{h,p^-}(\mathcal{T}_h) \subset \Lambda^k_{h,p}(\mathcal{T}_h)$. The polynomial interpolation order p has to be chosen such that the consistency error does not destroy the accuracy order related to the finite element approximation. Moreover, in view of (2.9), the characterization (2.11) automatically incorporates an upwinding of the Lie derivative. Lastly, since $\mathbf{u}$ is Lipschitz continuous and the discrete differential forms

are piecewise polynomials, the moments of the contracted forms on each j-cell of $\mathcal{T}_h$ are well-defined from within the d-cell in the upwind direction of the flow.

As a result of the discretization of the Lie derivative, the discrete advection problem, recast in weak form, reads: Find $\omega_h \in \Lambda^k_{h,r}(\mathcal{T}_h)$ such that

$$a_h(\omega_h, \eta_h) = (f, \eta_h)_\Omega, \qquad \forall\, \eta_h \in \Lambda^k_{h,r}(\mathcal{T}_h), \tag{2.12}$$

where the bilinear form $a_h(\cdot,\cdot)$ is defined, for all ω_h, $\eta_h \in \Lambda^k_{h,r}(\mathcal{T}_h)$, as

$$a_h(\omega_h, \eta_h) := (\alpha\omega_h, \eta_h)_\Omega + \int_\Omega (\mathcal{I}^k_{\mathbf{u},p}(\mathsf{i}_\mathbf{u}\mathsf{d}^k\omega_h) \wedge \star\eta_h + \mathsf{d}^{k-1}\mathcal{I}^{k-1}_{\mathbf{u},p^-}(\mathsf{i}_\mathbf{u}\omega_h) \wedge \star\eta_h).$$

Remark 2.4 (Boundary conditions at the inflow boundary)**.** Incorporating the boundary conditions in the discrete definition of the Lie derivative for k-forms requires the computation of the moment-based degrees of freedom at the boundary j-cells, $k \le j \le M^{p,k}_{\min}$. Note that the trace of the form and the trace of its contraction, $\mathrm{tr}(\mathsf{i}_\mathbf{n}\omega_h)$, at the inflow boundary of the domain are supplied by the boundary conditions. One can decompose the velocity field $\mathbf{u}$ in its normal component $\mathbf{u_n} := (\mathbf{u}\cdot\mathbf{n})\mathbf{n}$ and its tangential component $\mathbf{u_t} := (\mathbf{n}\times\mathbf{u})\times\mathbf{n}$, such that

$$\mathsf{i}_\mathbf{u}\omega_h = \mathsf{i}_{\mathbf{u_n}}\omega_h + \mathsf{i}_{\mathbf{u_t}}\omega_h = (\mathbf{u}\cdot\mathbf{n})\mathsf{i}_\mathbf{n}\omega_h + \mathsf{i}_{\mathbf{u_t}}\omega_h, \qquad \forall\,\omega_h \in \Lambda^k_h(\mathcal{T}_h),\ \forall\, k.$$

Note that the contraction by the tangential component of the velocity is available from the trace of ω_h (2.4). However, in the case of non-smooth boundaries, the contraction might not be uniquely defined at a given boundary j-cell, $j \le d-1$. One could average the contributions from the d-cells sharing the j-cell. For example, in two dimensions, at a boundary node $\mathbf{x} \in \Delta_0(\mathcal{T}_h)\cap\partial\Omega$ such that $\mathbf{x} \in \Delta_0(e_1)\cap\Delta_0(e_2)$ for some edges $e_1, e_2 \in \Delta_1(\mathcal{T}_h)\cap\partial\Omega$, one can approximate the contraction of a 1-form ω_h as

$$\mathsf{i}_\mathbf{u}\omega_h \approx \frac{1}{2}((\mathbf{u}\cdot\mathbf{n}_1)\mathsf{i}_{\mathbf{n}_1}\omega_h + \mathsf{i}_{\mathbf{u_t}_1}\omega_h) + \frac{1}{2}((\mathbf{u}\cdot\mathbf{n}_2)\mathsf{i}_{\mathbf{n}_2}\omega_h + \mathsf{i}_{\mathbf{u_t}_2}\omega_h).$$

2.3.1 Discrete Lie Derivative in Terms of Vector Proxies

We report the vector proxy representation of the discrete Lie derivative defined in (2.11). Let V_h be finite element spaces of vector proxies associated with the spaces $\Lambda^k_{h,r}(\mathcal{T}_h)$ of polynomial differential k-forms of degree at most $r \ge 1$ on the three-dimensional cellular complex $\mathcal{T}_h$. Let $\mathcal{I}^k_{\mathbf{u},p}$, $0 \le k \le 2$, and $\mathcal{I}^k_{\mathbf{u},p^-}$, $1 \le k \le 3$, be upwind interpolation operators onto piecewise polynomial spaces of degree at most $p \ge 1$ and $p^- \ge 1$, respectively. Let $w_h \in V_h$ or $\mathbf{w}_h \in V_h$ be the vector proxy representation of the k-form $\omega_h \in \Lambda^k_{h,r}(\mathcal{T}_h)$ and let $M^{p,k}_{\min}$ be defined as in (2.7) for $d = 3$. The discrete Lie derivative (2.11) reads

$$\begin{aligned} k=0: \qquad \mathrm{L}^h_\mathbf{u} w_h &= \mathcal{I}^0_{\mathbf{u},p}(\mathsf{i}_\mathbf{u}\mathsf{d}^0 w_h) = \mathcal{I}^0_{\mathbf{u},p}(\mathbf{u}\cdot\mathrm{grad} w_h) \\ &= \sum_{j=0}^{M^{p,0}_{\min}} \sum_{f_j\in\Delta_j(\mathcal{T}_h)} \sum_{\ell=1}^{N_j} W^\ell_{f_j}(\mathbf{u}\cdot\mathrm{grad} w_{h|_{T^{\mathsf{upw}}_{f_j}}})\,\lambda^\ell_j, \end{aligned} \tag{2.13}$$

where $\{\lambda^\ell_j\}_{j,\ell}$ is a basis of H^1-conforming polynomials of degree at most p.

Let $\{\phi^\ell_j\}_{j,\ell}$ be a basis of $\mathrm{H}(\mathbf{curl},\Omega)$-conforming polynomials of degree at most p and $\{\lambda^\ell_j\}_{j,\ell}$ a basis of H^1-conforming polynomials of degree at most p^-. There holds,

$$\begin{aligned} k=1: \qquad \mathrm{L}^h_\mathbf{u}\mathbf{w}_h &= \mathcal{I}^1_{\mathbf{u},p}(\mathsf{i}_\mathbf{u}\mathsf{d}^1\mathbf{w}_h) + \mathsf{d}^0\,\mathcal{I}^0_{\mathbf{u},p^-}(\mathsf{i}_\mathbf{u}\mathbf{w}_h) = \mathcal{I}^1_{\mathbf{u},p}(\mathbf{curl}\,\mathbf{w}_h\times\mathbf{u}) + \mathrm{grad}(\mathcal{I}^0_{\mathbf{u},p^-}(\mathbf{u}\cdot\mathbf{w}_h)) \\ &= \sum_{j=1}^{M^{p,1}_{\min}} \sum_{f_j\in\Delta_j(\mathcal{T}_h)} \sum_{\ell=1}^{N_j} W^\ell_{f_j}(\mathbf{curl}\,\mathbf{w}_h\times\mathbf{u}_{|_{T^{\mathsf{upw}}_{f_j}}})\,\phi^\ell_j \\ &\quad + \sum_{j=0}^{M^{p^-,0}_{\min}} \sum_{f_j\in\Delta_j(\mathcal{T}_h)} \sum_{\ell=1}^{N_j} W^\ell_{f_j}(\mathbf{u}\cdot\mathbf{w}_{h|_{T^{\mathsf{upw}}_{f_j}}})\,\mathrm{grad}\lambda^\ell_j. \end{aligned}$$

Let $\{\varphi_j^\ell\}_{j,\ell}$ be a basis of $\mathrm{H}(\mathrm{div},\Omega)$-conforming polynomials of degree at most p and $\{\phi_j^\ell\}_{j,\ell}$ a basis of $\mathrm{H}(\mathbf{curl},\Omega)$-conforming polynomials of degree at most p^-, then

$$\begin{aligned} k=2: \qquad \mathrm{L}^h_{\mathbf{u}}\mathbf{w}_h &= \mathcal{I}^2_{\mathbf{u},p}(\mathsf{i}_{\mathbf{u}}\mathsf{d}^2\mathbf{w}_h) + \mathsf{d}^1\,\mathcal{I}^1_{\mathbf{u},p^-}(\mathsf{i}_{\mathbf{u}}\mathbf{w}_h) = \mathcal{I}^2_{\mathbf{u},p}(\mathbf{u}\,\mathrm{div}\mathbf{w}_h) + \mathbf{curl}\,(\mathcal{I}^1_{\mathbf{u},p^-}(\mathbf{w}_h\times\mathbf{u})) \\ &= \sum_{j=2}^{M^{p,2}_{\min}} \sum_{f_j\in\Delta_j(\mathcal{T}_h)} \sum_{\ell=1}^{N_j} W^\ell_{f_j}(\mathbf{u}\,\mathrm{div}\mathbf{w}_{h|_{T^{\mathsf{upw}}_{f_j}}})\,\varphi^\ell_j \\ &\quad + \sum_{j=1}^{M^{p^-,1}_{\min}} \sum_{f_j\in\Delta_j(\mathcal{T}_h)} \sum_{\ell=1}^{N_j} W^\ell_{f_j}(\mathbf{w}_h\times\mathbf{u}_{|_{T^{\mathsf{upw}}_{f_j}}})\,\mathbf{curl}\,\phi^\ell_j. \end{aligned}$$

For $\{\varphi_j^\ell\}_{j,\ell}$ basis of $\mathrm{H}(\mathrm{div},\Omega)$-conforming polynomials of degree at most p^-,

$$k=3: \qquad \mathrm{L}^h_{\mathbf{u}}w_h = \mathsf{d}^2\,\mathcal{I}^2_{\mathbf{u},p^-}(\mathsf{i}_{\mathbf{u}}w_h) = \mathrm{div}(\mathcal{I}^2_{\mathbf{u},p^-}(\mathbf{u}w_h)) = \sum_{j=2}^{M^{p^-,2}_{\min}} \sum_{f_j\in\Delta_j(\mathcal{T}_h)} \sum_{\ell=1}^{N_j} W^\ell_{f_j}(\mathbf{u}w_{h|_{T^{\mathsf{upw}}_{f_j}}})\,\mathrm{div}\varphi^\ell_j.$$

Remark 2.5 (Tabata's scheme)**.** Let $\mathcal{T}_h$ denote a simplicial triangulation of $\Omega\subset\mathbb{R}^d$ of weakly acute type. We consider the extrusion contraction upwind discretization of the scalar advection problem with linear Lagrangian finite element spaces V_h. Using the discrete Lie derivative (2.13) in the weak formulation (2.12), yields the bilinear form

$$a_h(w_h,v_h) = \sum_{\ell=1}^{N_0} \mathbf{u}(x_\ell)\cdot(\mathrm{grad}w_h)_{|_{T^{\mathsf{upw}}_{x_\ell}}}(x_\ell)\int_\Omega \lambda^\ell v_h, \qquad \forall\, w_h, v_h\in V_h.$$

where $\{\lambda^\ell\}_\ell$ are the barycentric coordinates and $N_0 := \dim V_h = \sharp\Delta_0(\mathcal{T}_h)$. Approximating the integration on Ω using local quadrature rules $Q(T) = \{a_{i,T}, q_{i,T}\}_{i=0}^d$ with weights $\{q_{i,T} = 1/(d+1)\}_i$ and nodes $\{a_{i,T}\}_i$ at the mesh 0-cells (vertices of the d-simplices), results in

$$\begin{aligned} a_h(w_h,v_h) &= \sum_{\ell=1}^{N_0} \mathbf{u}(x_\ell)\cdot(\mathrm{grad}w_h)_{|_{T^{\mathsf{upw}}_{x_\ell}}}(x_\ell) \sum_{T\in\mathcal{T}_h}\sum_{a_{i,T}\in\Delta_0(T)} q_{i,T}\lambda^\ell(a_{i,T})v_h(a_{i,T}) \\ &= \sum_{T\in\mathcal{T}_h}\sum_{a_{i,T}\in\Delta_0(T)} q_{i,T}\mathbf{u}(a_{i,T})\cdot(\mathrm{grad}w_h)_{|_{T^{\mathsf{upw}}_{a_{i,T}}}}(a_{i,T})v_h(a_{i,T}), \end{aligned}$$

and the so-called *upwind quadrature* or Tabata's scheme [60] is recovered. The method proposed by Tabata to solve the transient scalar advection-diffusion problem with homogeneous Dirichlet boundary conditions at the domain boundaries, is first order accurate, and it delivers an algebraic system M-matrix (i.e., a non-singular matrix whose entries $a_{i,j}$ satisfy $a_{i,j}\le 0$ for $i\neq j$ and the entries $b_{i,j}$ of the inverse matrix are non-negative, $b_{i,j}\ge 0$). This entails that the discrete solution operator is inverse monotone. Therefore, when augmented with a standard linear finite element discretization of the diffusion operator, the resulting scheme is able to preserve the inverse-monotonicity property and hence the maximum principle characterizing the problem at the continuous level [60, Theorem 1].

2.4 Commuting Property of the Discrete Lie Derivative

Owing to Cartan's formula, it can be easily verified that the exterior derivative and the Lie derivative commute, namely

$$\mathsf{d}^k\mathrm{L}_{\mathbf{u}}\omega = \mathrm{L}_{\mathbf{u}}\mathsf{d}^k\omega, \qquad \forall\,\omega\in\Lambda^k(\Omega)\,. \tag{2.14}$$

The commuting property has the fundamental consequence that closed differential forms are Lie advected into closed forms. In the MHD perspective, this translates into the exact preservation of the divergence constraint at every time. Moreover, it entails that, if $\omega\in\Lambda^k(\Omega)$ is solution of the advection problem for k-forms, then $\mathsf{d}^k\omega$ is solution of the advection problem for $(k+1)$-forms, under suitable forcing terms,

initial and boundary conditions. As an example, in three-dimensional ideal MHD flows, the magnetic potential $\mathbf{A}$ and the magnetic induction field, $\mathbf{B} = \mathbf{curl}\,\mathbf{A}$, satisfy the advection problem for the vector proxies of differential 1-forms and 2-forms, respectively.

The discretization of the Lie derivative proposed in (2.11) yields an advection operator satisfying the commuting property (2.14) in the discrete setting.

Proposition 2.6. *Let $\Omega \subset \mathbb{R}^d$ be a bounded Lipschitz domain and let $\mathcal{T}_h$ be a cellular complex on Ω. Let $p^+, r^+ \geq 1$ be such that $\mathsf{d}^k\,\Lambda^k_{h,p}(\mathcal{T}_h) \subset \Lambda^{k+1}_{h,p^+}(\mathcal{T}_h)$ and $\mathsf{d}^k\,\Lambda^k_{h,r}(\mathcal{T}_h) \subset \Lambda^{k+1}_{h,r^+}(\mathcal{T}_h)$, respectively, with $p, r \geq 1$. Let $\mathbf{u} \in W^{1,\infty}(\Omega)$ and let $\mathrm{L}^h_{\mathbf{u}}$ be the extrusion contraction upwind discretization of the Lie derivative $\mathrm{L}_{\mathbf{u}}$ in (2.11). For all $0 \leq k \leq d-1$, the following diagram*

$$\begin{array}{ccc} \Lambda^k_{h,r}(\mathcal{T}_h) & \xrightarrow{\mathsf{d}^k} & \Lambda^{k+1}_{h,r^+}(\mathcal{T}_h) \\ \downarrow{\scriptstyle \mathrm{L}^h_{\mathbf{u}}} & & \downarrow{\scriptstyle \mathrm{L}^h_{\mathbf{u}}} \\ \Lambda^k_{h,p}(\mathcal{T}_h) & \xrightarrow{\mathsf{d}^k} & \Lambda^{k+1}_{h,p^+}(\mathcal{T}_h), \end{array}$$

commutes, namely, $\mathrm{L}^h_{\mathbf{u}}\mathsf{d}^k\omega_h = \mathsf{d}^k\mathrm{L}^h_{\mathbf{u}}\omega_h$, for all $\omega_h \in \Lambda^k_{h,r}(\mathcal{T}_h) \subset H\Lambda^k(\Omega)$.

Proof. The commutativity of the discrete exterior and Lie derivatives follows immediately from the topological properties of the (discrete) exterior derivative. Indeed, if $\omega_h \in \Lambda^k_{h,r}(\mathcal{T}_h)$, the definition of discrete Lie derivative in (2.11) results in

$$\begin{aligned} \mathrm{L}^h_{\mathbf{u}}\mathsf{d}^k\omega_h = \mathcal{I}^{k+1}_{\mathbf{u},p^+}(\mathsf{i}_{\mathbf{u}}\mathsf{d}^{k+1}\mathsf{d}^k\omega_h) + \mathsf{d}^k\,\mathcal{I}^k_{\mathbf{u},p}(\mathsf{i}_{\mathbf{u}}\mathsf{d}^k\omega_h) &= \mathsf{d}^k(\mathcal{I}^k_{\mathbf{u},p}(\mathsf{i}_{\mathbf{u}}\mathsf{d}^k\omega_h)) \\ &= \mathsf{d}^k(\mathsf{d}^{k-1}\,\mathcal{I}^{k-1}_{\mathbf{u},p^-}(\mathsf{i}_{\mathbf{u}}\omega_h) + \mathcal{I}^k_{\mathbf{u},p}(\mathsf{i}_{\mathbf{u}}\mathsf{d}^k\omega_h)) = \mathsf{d}^k\mathrm{L}^h_{\mathbf{u}}\omega_h, \end{aligned}$$

owing to the fact that the discrete exterior derivative satisfies $\mathsf{d}^{k+1} \circ \mathsf{d}^k = 0$. □

The result of Proposition 2.6 has two major consequences. Under the assumption of unique solvability of the discrete time-dependent problem corresponding to (2.12), discrete closed k-forms are Lie advected into closed k-forms. Consider the semi-discrete problem $\partial_t\omega_h + \alpha\omega_h + \mathrm{L}^h_{\mathbf{u}}\omega_h = f$, and suppose the initial datum is a closed form. From an algebraic perspective, let $\mathbb{L}$ be the matrix associated with the discretization of the Lie derivative (2.11). Let W^n be the vector of degrees of freedom for ω_h at time t^n. In the simplest case of explicit Euler timestepping, $\mathbb{M}W^{n+1} = \mathbb{M}W^n - \Delta t^n\,\alpha\mathbb{M}W^n - \Delta t^n\mathbb{L}W^n + \Delta t^n F^n$, where $\mathbb{M}$ is the mass matrix and F^n is the load vector associated with the source term at time t^n. By Proposition 2.6, the incidence matrix $\mathbb{D}^k$, representing the exterior derivative operator, commutes with $\mathbb{L}$. Hence, under suitable boundary conditions, $\mathbb{D}^kW^n = 0$ for all $n \geq 1$, provided the right hand side is closed at all times. Secondly, the polynomial spaces $\mathcal{P}^-_r\Lambda^k(\mathcal{T}_h)$ and $\mathcal{Q}^-_r\Lambda^k(\mathcal{T}_h)$ form long exact sequences for a fixed polynomial degree $r \geq 1$ [4, Section 3.5]. If a priori convergence results (in a certain norm) independent of the form degree k can be established, then, upon suitably tuning the polynomial approximation and interpolation orders, no accuracy is lost in solving the advection problem for the magnetic potential, rather than the magnetic induction advection.

3 Extended Euler Equations

The local splitting of the MHD system into two systems with discontinuous coefficients yields an advection problem for the magnetic induction/potential with a known discontinuous velocity field and the conservation laws for the fluid variables with the $\mathbf{B}$ field treated as a discontinuous known function. The second block of the MHD system (1.1), the extended Euler system, consists of the conservation equations for mass, momentum and (hydrodynamic) energy with the magnetic induction field entering through the Lorentz force, namely

$$\begin{cases} \partial_t\rho + \mathrm{div}(\rho\mathbf{u}) = 0, \\ \partial_t(\rho\mathbf{u}) + \mathbf{div}\,(\rho\mathbf{u}\otimes\mathbf{u} + p\mathbb{I}) = \mathbf{J}\times\mathbf{B}, \\ \partial_t E^{\mathrm{hd}} + \mathrm{div}\left(\left(E^{\mathrm{hd}} + p\right)\mathbf{u}\right) = \mathbf{J}\cdot\mathbf{E}, \end{cases} \tag{3.1}$$

where E^{hd} denotes the hydrodynamic energy, sum of the thermal and kinetic energies. Using Maxwell's equations for perfectly conducting fluids to express the current $\mathbf{J}$ and the electric field $\mathbf{E}$, the extended Euler system reduces to the fluid part of the ideal MHD equations (1.1a), (1.1b) and (1.1c), see e.g. [52, Section 6.1] for a detailed derivation.

The extended Euler system is a *parametric* hyperbolic system of conservation laws. In three dimensions, if $\mathbf{U} := (\rho, \rho u^1, \rho u^2, \rho u^3, E)$ denotes the vector of the conserved fluid variables, and $\mathbf{x} = (x^1, x^2, x^3) \in \mathbb{R}^3$, then (3.1) can be written in flux form according to (1.1) as

$$\partial_t \mathbf{U} + \sum_{\ell=1}^{3} \partial_{x^\ell} f^\ell(\mathbf{U}, \mathbf{B}) = \mathbf{0}. \tag{3.2}$$

If $\delta_{i,\ell}$ denotes the Kronecker delta, the directional fluxes $\{f^\ell\}_{\ell=1}^3$ are defined as

$$f^\ell(\mathbf{U}, \mathbf{B}) = \begin{pmatrix} \rho u^\ell \\ \rho u^1 u^\ell - B_1 B_\ell + \left(p + \frac{1}{2}\|\mathbf{B}\|_{\ell^2}^2\right) \delta_{1,\ell} \\ \rho u^2 u^\ell - B_2 B_\ell + \left(p + \frac{1}{2}\|\mathbf{B}\|_{\ell^2}^2\right) \delta_{2,\ell} \\ \rho u^3 u^\ell - B_3 B_\ell + \left(p + \frac{1}{2}\|\mathbf{B}\|_{\ell^2}^2\right) \delta_{3,\ell} \\ \left(E + p + \frac{1}{2}\|\mathbf{B}\|_{\ell^2}^2\right) u^\ell - (\mathbf{u}\cdot\mathbf{B}) B_\ell \end{pmatrix}.$$

The extended Euler equations form a weakly hyperbolic system of conservation laws. The eigenvalues of the directional Jacobian can be derived as in [22, Section 2.1], and are given by

$$\lambda^1 = \mathbf{u}\cdot\mathbf{n} - \mathbf{u}^{\mathrm{E}}\cdot\mathbf{n}, \qquad \lambda^{2,3,4} = \mathbf{u}\cdot\mathbf{n}, \qquad \lambda^5 = \mathbf{u}\cdot\mathbf{n} + \mathbf{u}^{\mathrm{E}}\cdot\mathbf{n}, \tag{3.3}$$

where $\mathbf{u}^{\mathrm{E}} := (a^{\mathrm{E},1}(\mathbf{V},\mathbf{B}), a^{\mathrm{E},2}(\mathbf{V},\mathbf{B}), a^{\mathrm{E},3}(\mathbf{V},\mathbf{B}))$ and $a^{\mathrm{E},\ell}$ denotes the sound speed of the acoustic wave in the ℓ-direction

$$a^{\mathrm{E},\ell}(\mathbf{V},\mathbf{B}) = \frac{1}{\sqrt{\rho}} \sqrt{\gamma p n_\ell + (\gamma - 1)\left[n_\ell(\|\mathbf{B}\|_{\ell^2}^2 - B_\ell^2) - B_\ell(\mathbf{B}\cdot\mathbf{n} - B_\ell n_\ell)\right]}, \qquad \ell \in \{1,2,3\}. \tag{3.4}$$

The Riemann solution of the extended Euler system is then characterized by five waves: two acoustic waves, rarefactions/shocks moving to the left/right and a shear wave.

3.1 Finite Volume Discretization

For the numerical discretization of the extended Euler problem, we design, in the present section, finite volume schemes using reduced waves approximate Riemann solvers as in [22, Section 2.1].

Hereafter we restrict to Cartesian domains $\Omega = J_1 \times \ldots \times J_d \subset \mathbb{R}^d$, with $J_\ell \subset \mathbb{R}$, $\ell = 1, \ldots, d$, bounded and connected. We proceed via a *dimensional splitting* by designing numerical discretizations of one-dimensional problems in each space direction and combining the solutions thus obtained. Let $\{\mathcal{T}_h\}_h$ be a family of partitions of Ω obtained, for all $h > 0$, as $\mathcal{T}_h = \mathcal{T}_{h_1}^1 \times \ldots \times \mathcal{T}_{h_d}^d$, where $\mathcal{T}_{h_\ell}^\ell$ is a uniform mesh on J_ℓ with $M_h^\ell := \sharp\mathcal{T}_{h_\ell}^\ell$ elements. Hence, the mesh width in the ℓ-direction is given by $h_\ell = |J_\ell|/M_h^\ell$ and $h = \max_\ell h_\ell$. Every control volume $T_{\mathfrak{j}} \in \mathcal{T}_h$ is identified by its barycenter $\mathbf{x}_{\mathfrak{j}} = (x_{j_1}^1, \ldots, x_{j_d}^d)$, where $\mathfrak{j} = (j_1, \ldots, j_d)$ is a multi-index in $\mathfrak{J} := \mathbb{N}^d \cap ([1, M_h^1] \times \ldots \times [1, M_h^d])$, which "selects" the spatial direction. The $(d-1)$-skeleton of the mesh is fundamental in determining the fluxes: the interfaces of the element $T_{\mathfrak{j}} \in \mathcal{T}_h$ are denoted by $\mathbf{x}_{\mathfrak{j}+\frac{1}{2}\mathbf{e}_{\mathfrak{t}}}$ where $\mathbf{e}_{\mathfrak{t}}$ is the $\mathfrak{t}$-th unit vector in $\mathbb{R}^d$. The weak solution $\mathbf{U}(\mathbf{x}, t)$ of the extended Euler system is approximated by cell averages,

$$\mathbf{U}(\mathbf{x},t)_{|_{T_{\mathfrak{j}}}} \approx \mathbf{U}_{\mathfrak{j}}(t) := \frac{1}{|T_{\mathfrak{j}}|} \int_{T_{\mathfrak{j}}} \mathbf{U}(\mathbf{x},t) d\mathbf{x}, \qquad \forall T_{\mathfrak{j}} \in \mathcal{T}_h,\ \mathfrak{j} \in \mathfrak{J}.$$

A semi-discrete finite volume scheme for the conservation law (3.2) on a fixed element $T_{\mathfrak{j}} \in \mathcal{T}_h$ is given by

$$\partial_t \mathbf{U}_{\mathfrak{j}}(t) = -\sum_{\ell=1}^{d} \frac{F^\ell_{\mathfrak{j}+\frac{1}{2}\mathbf{e}_\ell}(t) - F^\ell_{\mathfrak{j}-\frac{1}{2}\mathbf{e}_\ell}(t)}{h_\ell}, \qquad \forall\, \mathfrak{j} \in \mathfrak{J},$$

where $F^{\ell}_{\mathsf{j}+\frac{1}{2}\mathbf{e}_\ell}(t) = F^{\ell}_{\mathsf{j}+\frac{1}{2}\mathbf{e}_\ell}(\mathbf{B}(\mathbf{x}_{\mathsf{j}+\frac{1}{2}\mathbf{e}_\ell}, t), t)$ is a numerical flux consistent with the directional flux f^ℓ for all $1 \le \ell \le d$.

For the temporal discretization we rely on explicit *strong-stability preserving* Runge–Kutta (SSP-RK) schemes [27]. Let the temporal interval I be divided into subintervals $I = \bigcup_{n=0}^{N-1}(t^n, t^{n+1}]$, $N \in \mathbb{N}$, with $t^{n+1} = t^n + \Delta t^n$. Concerning the choice of the time step, we adopt a perspective where the extended Euler equations are considered as embedded in the physics of the full ideal MHD system. Since in MHD the fast magnetosonic waves propagate on a time scale much faster than the fluid velocity, these waves dictate the time step restrictions necessary for a stable numerical update. For the temporal discretization of the extended Euler system, the n-th time step is taken to be

$$\Delta t^n = C_{\mathsf{CFL}} \left(\sum_{\ell=1}^{d} \frac{\lambda^{\ell}_{\max}}{h_\ell} \right)^{-1},$$

where $C_{\mathsf{CFL}} > 0$ is a constant and $\{\lambda^{\ell}_{\max}\}_{\ell=1}^{d}$ are the maximum eigenvalues associated with the fast magnetosonic waves (1.2), namely

$$\lambda^{\ell}_{\max} = \max_{\mathsf{j}\in\mathfrak{J}} \lambda_f^{\mathrm{M},\ell}(\mathbf{U}^n_{\mathsf{j}}, \mathbf{B}^n_{\mathsf{j}}) := \max_{\mathsf{j}\in\mathfrak{J}} (|u^{\ell,n}_{\mathsf{j}}| + c_f^{\mathrm{M},\ell}(\mathbf{U}^n_{\mathsf{j}}, \mathbf{B}^n_{\mathsf{j}})), \qquad \ell = 1, \dots, d,$$

$$c_f^{M,\ell} = \frac{1}{\sqrt{2}} \sqrt{a^2 + \frac{\|\mathbf{B}\|^2_{\ell^2}}{\rho} + \sqrt{\left(a^2 + \frac{\|\mathbf{B}\|^2_{\ell^2}}{\rho}\right)^2 - 4a^2 \frac{B^2_\ell}{\rho}}}, \qquad \ell = 1, \dots, d.$$

3.1.1 Approximate Riemann Solvers

The use of Roe-type linearized Riemann solvers for MHD was pioneered by Brio and Wu [12] and further developed in [13]. However, the cumbersome computational cost and the failure of providing positivity preserving schemes [19] has thwarted the extensive application of linearized Roe-type solver in MHD simulations. An attractive alternative is provided by reduced-wave nonlinear solvers, the so-called *HLL solvers*, which approximate the wave structure of the full Riemann problem by a simplified set of known waves. Several HLL schemes for ideal MHD have been developed, e.g. in [30], in [10] (the so-called relaxed HLLC solver), in [49] (the HLLD solver) and in [46]. The HLL solvers combine limited computational cost, accurate reproduction of the physical features of the flow, and robustness of the resulting numerical scheme, although no HLL solver has the resolution of the Roe solver. We present HLL-type approximate Riemann solvers for the extended Euler equations based on solvers developed for the ideal MHD system. Each Riemann solver is specified only in the $x := x^1$-direction; modifications in other directions are derived likewise. For the sake of better readability, the superscript $\ell = 1$ is omitted and we switch from the multi-index j to the index i treating the problem as one-dimensional.

Two-wave HLL Solver. The Harten–Lax–van Leer (HLL) approximate Riemann solver, introduced in [32] for the inviscid gas dynamic equations, assumes a wave configuration for the Riemann problem solution consisting of three constant states separated by two shock waves moving to the left and to the right of the interface. The resulting HLL flux solver at time t^n is

$$F^{n,\mathrm{HLL}}_{i+1/2} = F(\mathbf{U}^n_i, \mathbf{U}^n_{i+1}, \mathbf{B}^n_{i+1/2}) = \begin{cases} f(\mathbf{U}^n_i, \mathbf{B}^n_{i+1/2}) & \text{if } s^L_{i+1/2} > 0, \\ f^{*,\mathrm{HLL}}_{i+1/2} & \text{if } s^L_{i+1/2} < 0 < s^R_{i+1/2}, \\ f(\mathbf{U}^n_{i+1}, \mathbf{B}^n_{i+1/2}) & \text{if } s^R_{i+1/2} < 0. \end{cases}$$

The selection of the left $s^L_{i+1/2}$ and right $s^R_{i+1/2}$ acoustic wave speeds determines different variants of the approximate flux. The middle flux $f^{*,\mathrm{HLL}}_{i+1/2}$ is determined, together with the intermediate subsonic state $\mathbf{U}^*_{i+1/2}$, by applying local conservation through Rankine–Hugoniot conditions, namely

$$f(\mathbf{U}^n_{i+1}, \mathbf{B}^n_{i+1/2}) - f^{*,\mathrm{HLL}}_{i+1/2} = s^R_{i+1/2}(\mathbf{U}^n_{i+1} - \mathbf{U}^*_{i+1/2}),$$
$$f^{*,\mathrm{HLL}}_{i+1/2} - f(\mathbf{U}^n_i, \mathbf{B}^n_{i+1/2}) = s^L_{i+1/2}(\mathbf{U}^*_{i+1/2} - \mathbf{U}^n_i).$$

Note that the computation of the flux $f(\mathbf{U}_i^n, \mathbf{B}_{i+1/2}^n)$ requires the knowledge of both the tangential and normal components of the $\mathbf{B}$ field at the interface. Whenever one of these quantities is not uniquely defined, we will take the arithmetic average $\{B^1\}_{i+1/2}$ and/or $\{B^2\}_{i+1/2}$ across the interface.

To determine the right and left speeds, Einfeldt suggested in [18] to use the minimum and maximum eigenvalues of a Roe average to restrain the spreading of contact discontinuities and increase the resolution at isolated shocks:

$$\begin{aligned} s_{i+1/2}^L &:= \min\{u_i^{1,n} - a^{\mathrm{E},1}(\mathbf{V}_i^n, \mathbf{B}_i^n), \{u^{1,n}\}_{i+1/2} - \widehat{a}^{\mathrm{E},1}(\{\mathbf{V}^n\}_{i+1/2}, \{\mathbf{B}^n\}_{i+1/2})\}, \\ s_{i+1/2}^R &:= \max\{u_{i+1}^{1,n} + a^{\mathrm{E},1}(\mathbf{V}_{i+1}^n, \mathbf{B}_{i+1}^n), \{u^{1,n}\}_{i+1/2} + \widehat{a}^{\mathrm{E},1}(\{\mathbf{V}^n\}_{i+1/2}, \{\mathbf{B}^n\}_{i+1/2})\}. \end{aligned} \tag{3.5}$$

The speed $a^{\mathrm{E},1}$ is defined as in (3.4). Lacking a Roe average for the extended Euler system, $\widehat{a}^{\mathrm{E},1}$ is taken as the "extended" sound speed

$$\begin{aligned} \{\rho^n (a^{\mathrm{E},1})^2\}_{i+1/2} &= \widehat{a}^{\mathrm{E},1}(\{\mathbf{V}^n\}_{i+1/2}, \{\mathbf{B}^n\}_{i+1/2}) \\ &= \sqrt{\frac{1}{\rho_i^n} + \frac{1}{\rho_{i+1}^n}} \sqrt{\gamma(p_i^n + p_{i+1}^n) + (\gamma - 1)[(B_2^n)_i^2 + (B_2^n)_{i+1}^2 + (B_3^n)_i^2 + (B_3^n)_{i+1}^2]}, \end{aligned}$$

associated with the averaged directional Jacobian

$$\widehat{A}_{i+1/2}^1 = \begin{pmatrix} \{u^{1,n}\}_{i+1/2} & \{\rho^n\}_{i+1/2} & 0 & 0 & 0 \\ 0 & \{u^{1,n}\}_{i+1/2} & 0 & 0 & \{1/\rho^n\}_{i+1/2} \\ 0 & 0 & \{u^{1,n}\}_{i+1/2} & 0 & 0 \\ 0 & 0 & 0 & \{u^{1,n}\}_{i+1/2} & 0 \\ 0 & \{\rho^n (a^{\mathrm{E},1})^2\}_{i+1/2} & \{\rho^n (a^{\mathrm{E},2})^2\}_{i+1/2} & \{\rho^n (a^{\mathrm{E},3})^2\}_{i+1/2} & \{u^{1,n}\}_{i+1/2} \end{pmatrix}.$$

Despite the efficiency and robustness of HLL-type Riemann solvers, the two-wave configuration hinders the resolution of physical features, in particular Alfvén and slow waves and contact discontinuities, yielding overdiffusive solutions.

Three-wave HLLC Solver. Contact discontinuities are "restored" in the modified HLL solver introduced by Toro, Spruce and Speares [61] and dubbed HLLC. The HLLC solver approximates the Riemann solution by three waves allowing for two intermediate states. The fast magnetosonic waves are modeled as in the HLL solver, whilst the intermediate states are separated by a wave moving with speed $s_{i+1/2}^M$ and modeling a contact discontinuity (associated with the multiple eigenvalue $\lambda^{2,3,4}$ (3.3)). The HLLC numerical flux is defined as

$$F_{i+1/2}^{n,\mathrm{HLLC}} = F(\mathbf{U}_i^n, \mathbf{U}_{i+1}^n, \mathbf{B}_{i+1/2}^n) = \begin{cases} f(\mathbf{U}_i^n, \mathbf{B}_{i+1/2}^n) & \text{if } s_{i+1/2}^L > 0, \\ f_L^* & \text{if } s_{i+1/2}^L < 0 < s_{i+1/2}^M, \\ f_R^* & \text{if } s_{i+1/2}^M < 0 < s_{i+1/2}^R, \\ f(\mathbf{U}_{i+1}^n, \mathbf{B}_{i+1/2}^n) & \text{if } s_{i+1/2}^R < 0. \end{cases}$$

The left and right speeds model the fast magnetosonic waves and are as in (3.5), the middle wave speed $s_{i+1/2}^M$ is the velocity of the averaged Jacobian $s_{i+1/2}^M = \{u^{1,n}\}_{i+1/2}$ since it models the contact discontinuity. The intermediate fluxes are determined by applying local conservation through the Rankine–Hugoniot conditions

$$\begin{aligned} s_{i+1/2}^L \mathbf{U}_L^* - f_L^* &= s_{i+1/2}^L \mathbf{U}_i^n - f(\mathbf{U}_i, \mathbf{B}_{i+1/2}^n), \\ s_{i+1/2}^M \mathbf{U}_L^* - f_L^* &= s_{i+1/2}^M \mathbf{U}_R^* - f_R^*, \\ s_{i+1/2}^R \mathbf{U}_{i+1}^n - f(\mathbf{U}_{i+1}^n, \mathbf{B}_{i+1/2}^n) &= s_{i+1/2}^R \mathbf{U}_R^* - f_R^*, \end{aligned} \tag{3.6}$$

where $\mathbf{U}_R^*$ and $\mathbf{U}_L^*$ denote the right and left intermediate states, respectively. Simple algebraic manipulations yield the intermediate fluxes f_R^* and f_L^*. However, since the system (3.6) is underdetermined, a further constraint on the intermediate states needs to be imposed. Linde suggested in [47, Section 4.3.3] to compute the jump of the intermediate states as a non-negative fraction of the initial jump across the middle wave, namely $\mathbf{U}_R^* - \mathbf{U}_L^* = \alpha(\mathbf{U}_i^n - \mathbf{U}_{i+1}^n)$ for $\alpha \in [0,1]$. If $c_* := |a^{\mathrm{E},1}(V_i^n, \mathbf{B}_i^n) - s_{i+1/2}^M|$, the choice

$$\alpha = \max\left\{0, 1 - \frac{s}{c_*}\right\}, \quad s := \frac{\|f(\mathbf{U}_{i+1}^n, \mathbf{B}_{i+1/2}^n) - f(\mathbf{U}_i^n, \mathbf{B}_{i+1/2}^n) - s_{i+1/2}^M(\mathbf{U}_{i+1}^n - \mathbf{U}_i^n)\|_{\ell^1}}{\left\|\mathbf{U}_{i+1}^n - \mathbf{U}_i^n\right\|_{\ell^1}},$$

aims at robustness of the Riemann solver together with good resolution of isolated shocks. As pointed out in [47], s gives an indication of the speed of the dominant wave in the frame of reference of the middle wave. Note that s can be in principle computed using a different norm.

3.1.2 Limitations of Finite Volume Schemes for the Extended Euler System

The formulation of approximate Riemann solvers for the extended Euler equations based on HLL-type solvers for the MHD Riemann problem is an attempt to capture the wave structure of the reduced problem viewed as a subset of the ideal MHD wave fan. However, the good properties of the aforementioned approximate Riemann solvers for the MHD system are not inherited straightforwardly by the extended Euler equations. As pointed out in [22], the lack of control on the $\mathbf{B}$ field and the unavailability of a Roe average, which consequently affects the choice of the wave speeds, do not guarantee that the resulting scheme is able to exactly capture fast magnetosonic shocks or isolated contact discontinuities. Analogously, with the $\mathbf{B}$ field resulting from the extrusion contraction approximation (2.11) of the magnetic advection problem for the magnetic field/potential, none of the foregoing solvers for the extended Euler system is provably positively conservative. Furthermore, the presence of the $\mathbf{B}$ field as a parameter entering the fluxes hinders the design of numerical fluxes satisfying a discrete version of the entropy inequality $\partial_t(\rho s) + \mathrm{div}(\rho \mathbf{u} s) \leq 0$, where $s := \log(p) - \gamma \log(\rho)$ is the thermodynamic entropy.

4 The FV-FEEC Schemes

The extrusion contraction upwind discretization derived in Section 2 for the magnetic induction equation and the finite volume schemes for the extended Euler system described in Section 3 can be combined in numerical schemes for the full ideal MHD problem, which we coin FV-FEEC (Finite Volume-Finite Element Exterior Calculus).

We implement a *synchronous* splitting, Algorithm 1, where the two systems, extended Euler and magnetic advection, are concurrently advanced in time, in the sense that after spatial discretization, the two problems are re-coupled to form a single system of ODEs. The latter is solved via explicit SSP Runge−Kutta timestepping. In this way, the coupling fields, the velocity and the magnetic induction, are updated within each subsystems at every intermediate stage of the temporal scheme.

Algorithm 1 Synchronous splitting algorithm

Set $n = 0$, $t = 0$. Given initial conditions $(\rho_0, \mathbf{u}_0, E_0, \mathbf{B}_0)$.
while time $t < T$ **do**
  $\mathbf{u}^{n;0} = \mathbf{u}^n$; $\mathbf{B}^{n;0} = \mathbf{B}^n$.
  for each step $1 \leq i \leq s$ of an s-stage SSP-RK timestepping **do**
    $\mathbf{u}^{n;i} \longleftarrow$ Solve the extended Euler equations given $\{\mathbf{B}^{n;j}\}_{j=0}^{i-1}$.
    $\mathbf{A}^{n;i} \longleftarrow$ Solve the advection of $(d-1)$-forms given $\{\mathbf{u}^{n;j}\}_{j=0}^{i-1}$.
    $\mathbf{B}^{n;i} \longleftarrow$ Compute the (discrete) curl of $\mathbf{A}^{n;i}$.
  end for
  $\mathbf{u}^{n+1} = \mathbf{u}^{n;s}$; $\mathbf{A}^{n+1} = \mathbf{A}^{n;s}$; $\mathbf{B}^{n+1} = \mathbf{B}^{n;s}$.
  Set $t = t + \Delta t^n$, $n = n + 1$.
end while

5 Numerical Experiments in Two Dimensions

This section is devoted to testing the new family of FV-FEEC schemes, for the two-dimensional planar MHD problem, on a set of numerical benchmark experiments. The aim is to provide numerical evidence of their accuracy, good stability properties and ability in preserving the physical distinctive features of the model at the continuous level. The two-dimensional setting provides a first step to assess the robustness of numerical schemes maintaining many of the physical features of the three-dimensional model and paves the way to three-dimensional simulations.

Lacking a stability and convergence theory for the extrusion contraction upwind schemes, we first test the method introduced in Section 2.2 for the transient advection problem. The aim is to derive empiric convergence properties in the L^2-norm and in some energy norm, and to look for numerical confirmation of the discrete commuting property stated in Proposition 2.6.

5.1 Numerical Tests: Extrusion Contraction

Since we are interested in the transient advection problem as part of the planar two-dimensional MHD model, we restrict to numerical simulations for the advection of 0-forms and 1-forms in two dimensions. Note that in this case the magnetic potential is a scalar function representing the transverse out-plane component of the three-dimensional vector magnetic potential, $\mathbf{B} = \mathbf{curl}_{2\mathrm{D}} A := (\partial_y A, -\partial_x A)^\top$.

5.1.1 Transient Advection of 0-Forms

On the domain $\Omega = [0,2]^2$ and on the time interval $I = [0,T] \subset \mathbb{R}$, $T > 0$, we consider the pure advection problem for the scalar magnetic potential A, namely

$$\begin{aligned} \partial_t A(t) + \mathbf{u} \cdot \mathrm{grad} A(t) = 0, \quad & \text{in } \Omega \times I, \\ A(0) = A_0, \quad & \text{in } \Omega, \end{aligned} \tag{5.1}$$

with periodic boundary conditions.

Test of Convergence: Constant Velocity. The initial condition $A_0 = \frac{1}{\pi}\cos(\pi y) + \frac{1}{2\pi}\cos(2\pi x)$ is advected at constant velocity $\mathbf{u} = (4,4)^\top$. On a family of Cartesian meshes $\{\mathcal{T}_h\}_h$, we consider the discrete variational formulation (2.12) with approximation spaces $\Lambda^k_{h,r}(\mathcal{T}_h)$ of bilinear ($r = 1$) and biquadratic ($r = 2$) Lagrangian finite elements. The polynomial degree of the upwind interpolation is chosen to coincide with the polynomial degree of the finite element trial and test spaces, that is $p = r$ in (2.13). In order to gauge the spatial accuracy of the extrusion contraction scheme, we use Heun timestepping with uniform time step $\Delta t = 0.1h$ for bilinear Lagrangian finite element approximations and $\Delta t = 0.01h$ for biquadratic Lagrangian finite elements. Owing to the periodicity of the domain, we can compare the numerical solution at final time $T = 0.5$ with A_0.

The projection of the numerical and exact solution at final time onto the one-dimensional line $\{\mathbf{x} \in \Omega,\ y = 1\}$ is shown in Figure 2, bottom row. The piecewise linear discretization yields a rather diffusive solution and first order accuracy in both the L^2- and H^1-norms, as reported in Figure 2 where the L^2-error of the potential A and of its two-dimensional **curl**, the magnetic induction field $\mathbf{B}$, is reported. Second order convergence is attained in the case of piecewise biquadratic discretization (and interpolation).

Orszag–Tang Benchmark with Given Velocity Field. We assess the performance of the extrusion contraction scheme in solving the more challenging MHD problem given by the Orszag–Tang vortex system [51] (see Section 5.3.3 for further details). We consider problem (5.1) with initial magnetic potential $A_0 = \frac{1}{\pi}\cos(\pi y) + \frac{1}{2\pi}\cos(2\pi x)$. The velocity field is supplied at each time step as the output of a high order finite volume discretization of the full ideal MHD system obtained with the ALSVID-UQ 3.0 (2014-03-20) code[1] (using a three-wave HLL solver and modified WENO reconstructions in order to keep the pressure and density positive).

The scalar advection problem is discretized in space on a Cartesian mesh using extrusion contraction piecewise linear and piecewise quadratic upwind schemes with velocity field averaged at the interpolation

[1] http://www.sam.math.ethz.ch/alsvid-uq (Accessed March 2016)

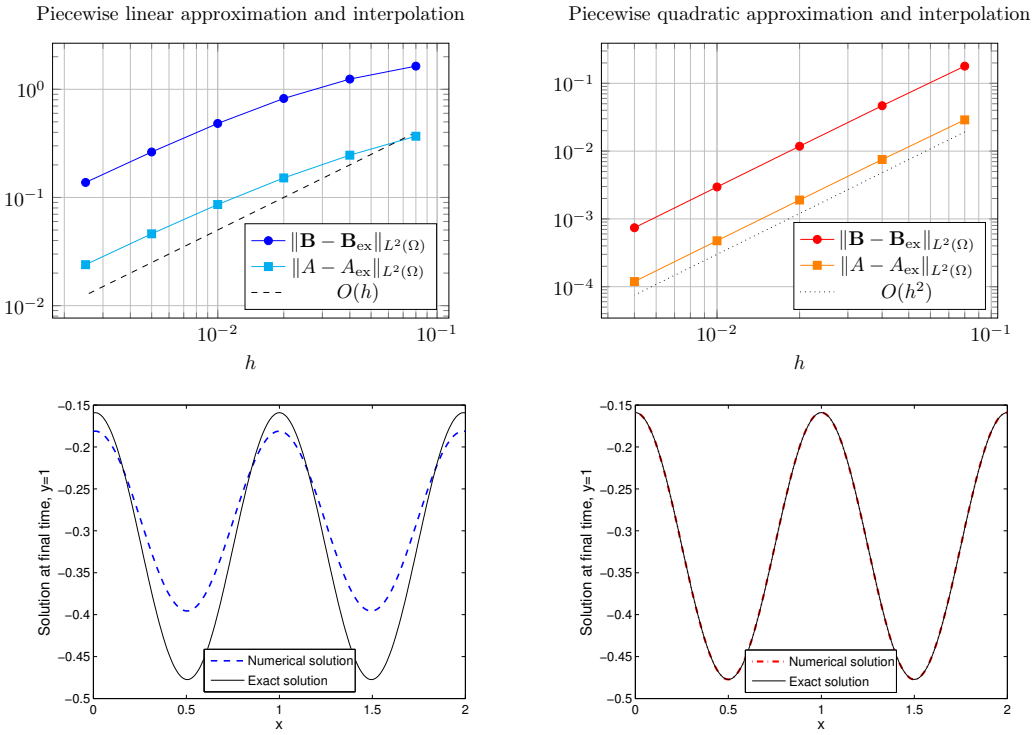

Figure 2: Test for advection of 0-forms with constant velocity. Convergence plot of the error in the L^2-norm at time $t = 0.5$ for the magnetic potential A and the induction field $\mathbf{B}$ (top row). The exact solution is $A_{\rm ex} \equiv A_0$ and analogous for the $\mathbf{B}$ field. Projection of the exact and numerical solution for $y = 1$ on a 200×200 Cartesian mesh (bottom row). Left: first order interpolation, bilinear Lagrangian finite elements. Right: second order interpolation, biquadratic Lagrangian finite elements.

nodes and upwind direction at each node given by the averaged velocity (in MHD flow simulations a more sophisticated approach to avoid the possible shortcoming of averaging the velocity values will be pointed out in Section 5.3). The polynomial order of the upwind interpolation operator coincides with the polynomial approximation degree. Heun timestepping is used for the temporal approximation on the time interval $I = [0, 1]$ with uniform time step $\Delta t = 5 \cdot 10^{-4}$.

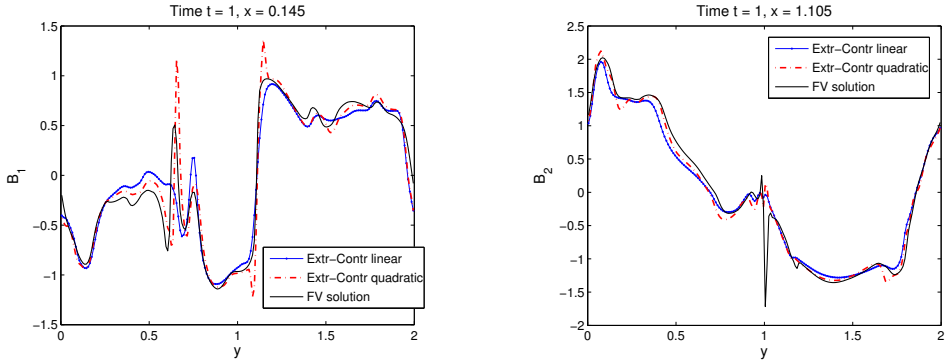

Figure 3: Orszag−Tang benchmark with given velocity field. Comparison plots of the projection of the $\mathbf{B}$ field for constant values of the x-coordinate on a Cartesian mesh with 200×200 elements. Discretization of the advection problem for 0-forms using piecewise linear and piecewise quadratic extrusion contraction upwind schemes. As reference solution, a high order finite volume solution of the full ideal MHD system obtained with the ALSVID-UQ code is considered.

The projection of the magnetic induction field, obtained with the foregoing discretizations, on lines

at constant x is compared with the reference finite volume discrete solution in Figure 3. As expected, the piecewise quadratic extrusion contraction approximation produces more accurate solutions than the piecewise linear discretization. However, it can be noticed that, near shocks and discontinuities, the piecewise quadratic solution exhibits "overshoots" and "undershoots". This is a typical by-product of numerical discretizations higher than first order accurate, as symptom of lack of monotonicity. We will comment on this issue later in Section 6.

5.1.2 Transient Advection of 1-Forms

On a simply connected bounded domain $\Omega \subset \mathbb{R}^2$ with Lipschitz boundary, we address the discretization of the initial boundary value problem describing the advection of the magnetic induction

$$\begin{aligned} \partial_t \mathbf{B} + \mathbf{u}\,\mathrm{div}\mathbf{B} + \mathrm{grad}^{\perp}(\mathbf{B}\cdot\mathbf{u}) &= \mathbf{f}, \quad && \text{in } \Omega \times I, \\ \mathbf{B}(0) &= \mathbf{B}_0, && \text{in } \Omega, \end{aligned} \tag{5.2}$$

with periodic boundary conditions and where $\perp$ denotes a clockwise rotation of $\pi/2$. We consider lowest order finite element approximations with finite element spaces of polynomial discrete differential forms of the first family, namely the rotated Raviart-Thomas elements [54].

Test of Convergence: Constant Velocity. The goal of this experiment is twofold: infer the possible accuracy of the scheme and verify that solenoidal vector fields are indeed advected into solenoidal vector fields, as asserted in Proposition 2.6. The magnetic advection problem (5.2) is considered on the domain $\Omega = [0,2]^2$ with periodic boundary conditions and in the time interval $I = [0, 0.5]$. The initial condition is set to $\mathbf{B}_0 = (-\sin(\pi y), \sin(2\pi x))^\top$, the advection velocity is constant $\mathbf{u} = (4,4)^\top$ and the forcing term is assumed to vanish, $\mathbf{f} = (0,0)^\top$. In view of the periodic boundary conditions, we compare the solution at final time with the initial condition. Figure 4 shows that the L^2-error converges at first order rate with respect to the mesh width h and the divergence of the magnetic induction field is maintained zero up to machine precision.

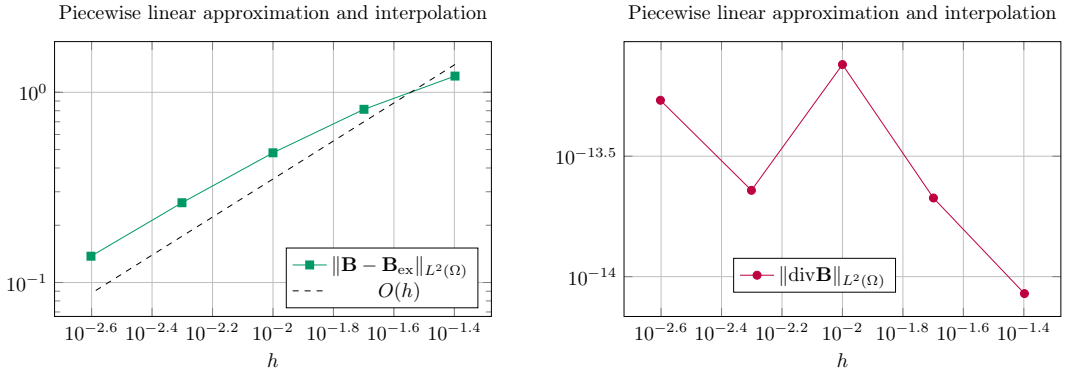

Figure 4: Test for advection of 1-forms with constant velocity. Convergence plot of the error in the L^2-norm at final time $T = 0.5$ (left). L^2-norm of the magnetic induction field (right). Piecewise linear extrusion contraction upwind schemes with Heun timestepping with uniform time step $\Delta t = 0.1h$.

Advection of Non-Solenoidal Magnetic Induction. As a second test case, we consider the advection of a magnetic induction field with non-zero divergence with the aim of monitoring the convergence rate of the solution in the L^2-norm and in the energy norm. On the unit square $\Omega = [0,1]^2$ with periodic boundary conditions and in the time interval $I = [0, 0.5]$, we consider the magnetic advection problem (5.2) with initial condition given by

$$\mathbf{B}_0 := \begin{cases} (\varphi, \varphi)^\top & \text{if } x^2 + (y - 0.25)^2 < 0.25, \\ (0,0)^\top & \text{otherwise,} \end{cases}$$

with $\varphi(x,y) := \cos(\pi\sqrt{x^2+(y-0.25)^2})^4$. The "hump" is Lie advected on the diagonal of the domain with velocity field $\mathbf{u} = (2,2)^\top$. The forcing term in this experiment is set to zero, $\mathbf{f} = (0,0)^\top$. We compute the numerical errors associated with the spatial discretization, at final time $T = 0.5$. Figure 5 shows that first order convergence is attained both in the L^2-norm and in the $\mathrm{H}(\mathrm{div},\Omega)$-seminorm.

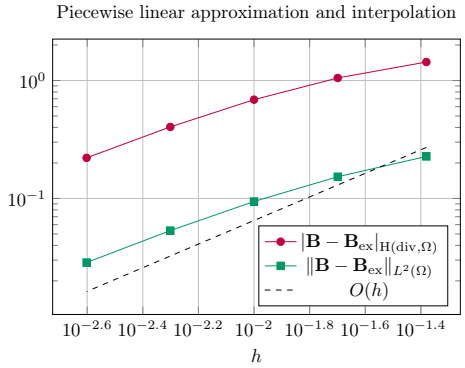

Figure 5: Advection of 1-forms. Non-solenoidal magnetic induction. Numerical convergence study of the piecewise linear extrusion contraction scheme. Heun timestepping with uniform time step $\Delta t = 0.1h$.

5.2 Numerical Experiments for Extended Euler

To experimentally gauge the performances of lowest order finite volume schemes for the extended Euler system derived in Section 3, we propose a two-dimensional MHD test with given magnetic induction field [7, Section 6]. More in details, the solution is smooth and known analytically at any point in space and time in the domain $\Omega \times I = [-5,5]^2 \times [0,0.5]$, see Section 5.3.1 for further details. Let $r(x,y,t) := \sqrt{(x-t)^2+(y-t)^2}$, the flow is characterized by the following set of data,

$$\rho(x,y,t) = 1, \quad p(x,y,t) = 1 + \frac{1}{8\pi}(\mu^2(1-r^2) - \kappa^2)e^{1-r^2},$$
$$\mathbf{u}(x,y,t) = (1,1)^\top + \frac{\kappa}{2\pi}e^{1/2(1-r^2)}(t-y, x-t)^\top.$$

The ratio of specific heats is $\gamma = 5/3$ and the parameters $\kappa = \mu = 1$. The magnetic induction field $\mathbf{B}$ is given at each time step in analytic form as $\mathbf{B}(x,y,t) = \frac{\mu}{2\pi}e^{1/2(1-r^2)}(t-y, x-t)^\top$. We aim at assessing the convergence properties of the scheme. Explicit Euler timestepping ($C_{\mathsf{CFL}} = 0.4$) is coupled with a piecewise constant finite volume discretization in space and tested with different approximate Riemann solvers. In Figure 6, the L^1-error of the primitive variables at final time $T = 0.5$ is reported. As expected, first order convergence is observed.

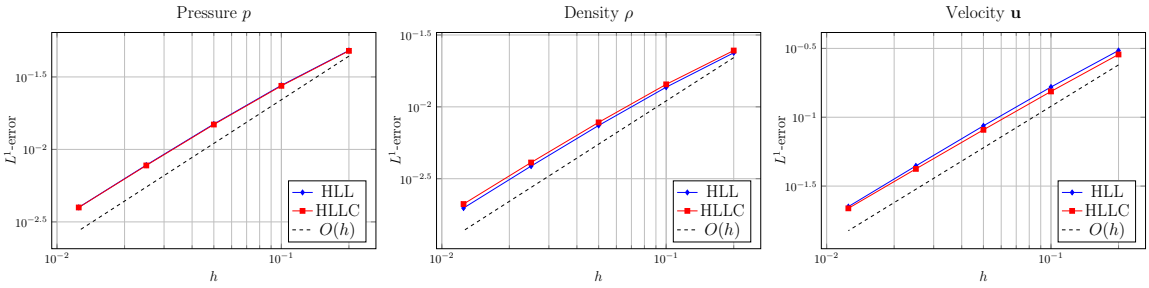

Figure 6: Smooth vortex. Accuracy test for finite volume discretizations of the extended Euler system with given analytic $\mathbf{B}$ field. Different approximate Riemann solvers are considered. In the legend, HLL refers to the two-wave Riemann solver with wave speeds as in (3.5) and HLLC to the three-wave Linde solver.

5.3 Numerical Experiments for Ideal MHD

In this section we numerically study the fully coupled FV-FEEC scheme described in Section 4 on a set of two-dimensional ideal MHD benchmark simulations. In particular, for the magnetic advection subproblem we focus on the potential-based formulation (2.1), for which extrusion contraction upwind schemes have been tested in Section 5.1.1.

Remark 5.1 (Collisional fluid velocities)**.** On a tensor product partition $\mathcal{T}_h$ of the computational domain Ω, the fluid velocity resulting from lowest order finite volume discretizations of the extended Euler equations is a $\mathcal{T}_h$-piecewise constant function $\mathbf{u} \in \mathcal{P}_0(\mathcal{T}_h)$ (collecting the cell averages of the fluid velocity in each mesh element). However, the extrusion contraction upwind discretization of the advection problem entails an upwind interpolation of the Lie derivative which requires the knowledge of the velocity field at the mesh nodes and along edges. One can approximate the value at a given node by averaging the values from the elements sharing the node. This pointwise interpolation might appear rather crude. It is especially the case in the presence of colliding or diverging velocity at a node or an edge where one might lose information on the local dynamics.

In MHD, the fast magnetosonic wave speed provides a good indicator of the flow dynamics. Hence, in the FV-FEEC algorithm implemented in the numerical experiments below, the upwind direction entering the discrete Lie derivative at the mesh cells where the velocity field is colliding or diverging is determined by the fast MHD wave speed (1.2), namely

$$c_f^M := (c_f^{M,1}, c_f^{M,2}), \quad \text{with} \quad c_f^{M,\ell} = \frac{1}{\sqrt{2}} \sqrt{a^2 + \frac{\|\mathbf{B}\|_{\ell^2}^2}{\rho} + \sqrt{\left(a^2 + \frac{\|\mathbf{B}\|_{\ell^2}^2}{\rho}\right)^2 - 4a^2 \frac{B_\ell^2}{\rho}}}, \quad \ell \in \{1,2\}.$$

Once the upwind direction has been uniquely identified at each mesh cell, the pointwise advection velocity at the nodes is taken from within the upwind element.

5.3.1 Accuracy Test: Smooth Vortex

In order to experimentally assess the accuracy of the lowest order FV-FEEC scheme, we present a genuinely two-dimensional (non-trivial) MHD test where the solution is known analytically at every point in space and time. The smooth vortex test was proposed in [7, Section 6] (a scaling factor $\sqrt{4\pi}$ has been absorbed in the definition of $\mathbf{B}$). The problem is associated with a smoothly varying fluid vortex which propagates at a $\pi/4$ angle to the computational mesh on the domain $\Omega = [-5,5]^2$ with periodic boundaries. The initial condition is given by a vortex characterized by fluctuations of the velocity and of the magnetic field, superimposed to an unperturbed MHD flow $\mathbf{U}_0 = (\rho_0, p_0, u_0^1, u_0^2) = (1,1,1,1)$, $\mathbf{B}_0 = \mathbf{0}$. Let $r(x,y,t) := \sqrt{(x-t)^2 + (y-t)^2}$, the flow is described by the following set of data,

$$\begin{aligned}
&\rho(x,y,t) = 1, \quad p(x,y,t) = 1 + \frac{1}{8\pi}(\mu^2(1-r^2) - \kappa^2)e^{1-r^2},\\
&\mathbf{u}(x,y,t) = \mathbf{u}_0 + \frac{\kappa}{2\pi} e^{1/2(1-r^2)}(t-y, x-t)^\top,\\
&\mathbf{B}(x,y,t) = \frac{\mu}{2\pi} e^{1/2(1-r^2)}(t-y, x-t)^\top, \quad A(x,y,t) = \frac{\mu}{2\pi} e^{1/2(1-r^2)}.
\end{aligned}$$

As initial datum we take $\mathbf{U}(\mathbf{x},0)$ with $\mathbf{u}_0 = (u_0^1, u_0^2)^\top = (1,1)^\top$, $\kappa = \mu = 1$ and $A(\mathbf{x},0)$ for the magnetic advection subproblem. The ratio of specific heats is $\gamma = 5/3$. The time interval is $I = [0, 0.5]$. Explicit Euler is used as timestepping with CFL constant $C_{\mathsf{CFL}} = 0.4$.

The numerical convergence study on smooth solutions in Figure 7 (left) displays first order convergence of the errors of the scalar magnetic potential in the norms associated with the Bochner spaces $L^\infty(I, L^2(\Omega))$ and $L^\infty(I, H^1(\Omega))$ and defined as $\|A\|_{L^\infty(I,H)} := \operatorname{ess\,sup}_{t\in I} \|A(t)\|_H$ on the Sobolev space $(H, \|\cdot\|_H)$. Analogous conclusions can be drawn from Figure 7 (right) where the $L^\infty(I, L^1(\Omega))$-errors of the $\mathcal{T}_h$-piecewise constant MHD primitive variables are illustrated.

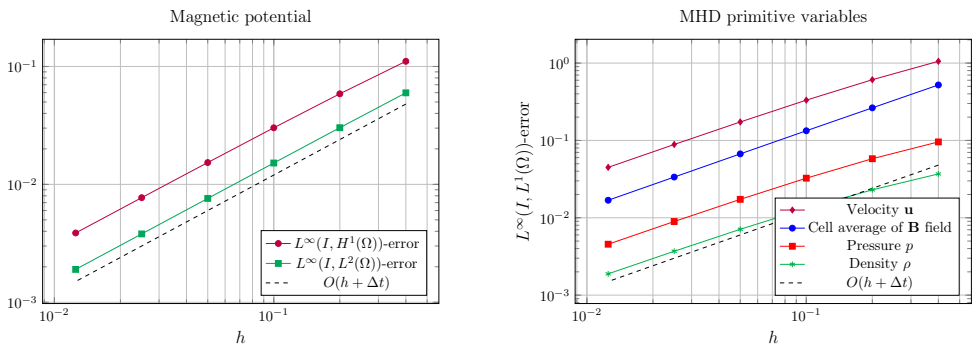

Figure 7: Accuracy test for full ideal MHD system. $L^\infty(I, L^2(\Omega))$- and $L^\infty(I, H^1(\Omega))$-error of the magnetic potential (left), $L^\infty(I, L^1(\Omega))$-error of the MHD primitive variables (right). Results obtained with piecewise constant finite volume discretizations of the extended Euler system with HLL Riemann solver and piecewise linear extrusion contraction scheme for the advection of the magnetic potential. Explicit Euler timestepping and $C_{\mathsf{CFL}} = 0.4$.

5.3.2 Super-Fast Expansion: Shock Tube Test

To the aim of testing the robustness of numerical schemes in delivering physically admissible solutions of the one-dimensional MHD equations, a super-fast expansion simulation has been used in e.g. [49, Section 6.1 p. 338] and [22, Section 3.2]. With the same goal, we study a variant of the foregoing test case in a formally two-dimensional setting. Let us consider the domain $\Omega = [0,1]^2$ with periodic upper $\{\mathbf{x} \in \Omega : y = 1\}$ and lower $\{\mathbf{x} \in \Omega : y = 0\}$ boundaries. In the remaining part of $\partial\Omega$, non-reflecting Neumann type boundary conditions are applied to the conserved variables of the extended Euler system, and outflow boundary conditions to the advection problem since the evolution of the velocity field does not induce any inflow boundary on the considered time interval $I = [0, 0.2]$. We perform planar two-dimensional simulations of the one-dimensional (in the x-direction) shock tube test with initial data

$$\begin{aligned}
&\rho_0(x,y) = 1, \quad p_0(x,y) = 0.45,\\
&u_0^1(x,y) = \begin{cases} -3.1 & \text{if } x < 0.5,\\ 3.1 & \text{if } x > 0.5, \end{cases} \qquad u_0^2(x,y) = 0,\\
&\mathbf{B}_0(x,y) = (0, 0.5)^\top, \quad A_0(x,y) = -0.5x,
\end{aligned}$$

and $\gamma = 5/3$ as ratio of specific heats. As the problem involves a left-moving and a right-moving rarefaction wave, the central region is subject to a super-fast expansion yielding very low density and pressure. In [22, Section 3.2], it has been observed that linearized Roe solvers for finite volume discretizations of the full MHD system usually run into negative pressure and density in such test case. The FV-FEEC scheme proves positively conservative at all tested resolutions, see Figure 8.

5.3.3 Orszag–Tang Benchmark

The so-called Orszag–Tang vortex system was introduced in [51, Section 3], and describes the transition to supersonic turbulence in the MHD equations. The development of shock waves and the complex interaction between various shocks with different speed, which characterized the solution, makes the Orszag–Tang benchmark a challenging test for numerical methods. Let us consider the domain $\Omega = [0, 2]^2$ with periodic boundary conditions. The time interval is $I = [0, 1]$. The initial conditions for the primitive fluid variables, the magnetic induction field $\mathbf{B}$ and the magnetic potential A are

$$\begin{aligned}
&\rho_0(x,y) = \gamma^2, \quad p_0(x,y) = \gamma, \quad \mathbf{u}_0(x,y) = (-\sin(\pi y), \sin(\pi x))^\top,\\
&\mathbf{B}_0(x,y) = (-\sin(\pi y), \sin(2\pi x))^\top, \quad A_0(x,y) = \frac{1}{\pi}\cos(\pi y) + \frac{1}{2\pi}\cos(2\pi x),
\end{aligned}$$

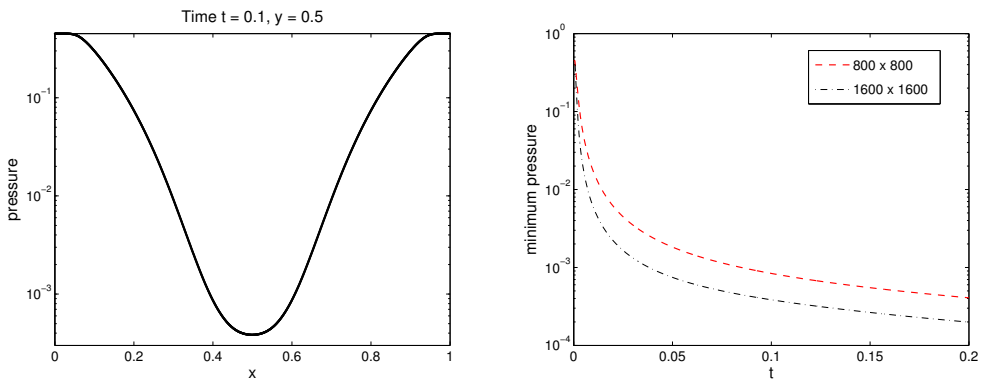

Figure 8: Super-fast expansion. Semi-logarithmic plot of the projection onto $\{\mathbf{x} \in \Omega : y = 0.5\}$ of the numerical pressure (left) at the intermediate time $t = 0.1$. Numerical discretization on a 1600×1600 Cartesian mesh with Heun timestepping and $C_{\mathsf{CFL}} = 0.4$. Lowest order extrusion contraction for the advection of the magnetic potential and finite volume scheme for the extended Euler equations using the HLL approximate Riemann solver. On the right, semi-logarithmic evolution plot of the minimum of the discrete pressure until time $t = 0.2$ at 800×800 and 1600×1600 mesh resolutions.

and $\gamma = 5/3$ is the gas constant. Since the Orszag−Tang test is a widely used benchmark, we can compare the performances of the FV-FEEC scheme with the numerical discretizations of [22]. As reported in [22, Section 3.3], finite volume schemes for the full MHD system based on Roe solvers, two-wave HLL and three-wave HLLC solvers, with and without divergence cleaning (via projection methods), experienced negative pressures at fine mesh resolution.

In Table 2, we compare the maximum pressure at final time $T = 1$ of the lowest order FV-FEEC discretization with the results reported in [22, Table 2.2] for the first order finite volume schemes HLL/SUS and HLLC/SUS from [22] and [20]. The reported values are comparable at all mesh resolutions: the HLLC solver for FV-FEEC gives slightly more "accurate" results, as experienced in Section 5.2 when testing approximate Riemann solvers on the extended Euler system, and shown in Figure 9 in comparison with a second order accurate reference solution[2].

$\sharp\mathcal{T}_h$	HLL/SUS [22, Table 2.2]	FV-FEEC HLL	HLLC/SUS [22, Table 2.2]	FV-FEEC HLLC
100×100	4.94	4.38	5.04	5.05
200×200	5.39	5.29	5.41	5.65
400×400	5.79	5.84	5.81	5.91
800×800	6.05	6.06	6.07	6.10
1600×1600	6.21	6.20	6.22	6.23

Table 2: Orszag−Tang benchmark. Maximum value of the discrete pressure at final time obtained with the FV-FEEC scheme with two-wave HLL and three-wave HLLC Riemann solvers, and compared with the values from the finite volume discretizations HLL(C)/SUS of [22].

Finite volume schemes are, by construction, conservative methods. However, the conservation property is not naturally inherited by the coupled FV-FEEC discretizations. In order to numerically assess the conservation properties of the FV-FEEC scheme, we monitor the evolution of the mean, on the computational domain Ω, of the conserved variables over time. Given the scalar function $f(\mathbf{x}, t)$ and the initial datum $f_0(\mathbf{x})$, we compute, on the partition of the temporal interval, the following error,

$$\mathcal{E}(f) := \max_{1 \le n \le N} |\overline{f}^n - \overline{f}_0|, \qquad \overline{f}^n := \fint_\Omega f(\mathbf{x}, t^n) d\mathbf{x} \quad \text{and} \quad \overline{f}_0 := \fint_\Omega f_0(\mathbf{x}) d\mathbf{x}. \tag{5.3}$$

[2]The reference solutions used throughout the present section were provided by R. Käppeli, SAM, ETH Zürich, and based on the FISH code [43].

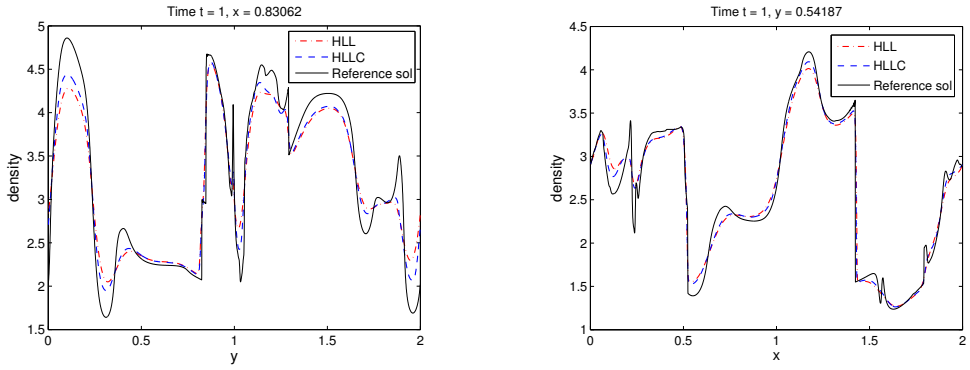

Figure 9: Orszag−Tang benchmark. Projections of the discrete density for constant values of the x-coordinate (left) and y-coordinate (right). Numerical discretization on a 1600×1600 Cartesian mesh. The finite volume scheme for the extended Euler equations is based on two-wave HLL and three-wave HLLC approximate Riemann solver. Heun timestepping with $C_{\mathsf{CFL}} = 0.4$. A second order accurate finite volume solution on 3200×3200 mesh elements is used as reference solution.

Whenever needed we consider the relative error $\mathcal{E}_r(f) := \mathcal{E}(f)/|\overline{f}_0|$. Table 3 reports the values of the aforementioned error on the conserved MHD variables and for different mesh refinements: perfect conservation.

$\sharp\mathcal{T}_h$	$\mathcal{E}_r(\rho)$	$\mathcal{E}(\rho u^1)$	$\mathcal{E}(\rho u^2)$	$\mathcal{E}(B_1)$	$\mathcal{E}(B_2)$	$\mathcal{E}_r(E)$
200×200	1.3097e−15	2.1723e−11	4.0363e−12	1.8402e−11	4.5034e−12	2.1552e−15
400×400	1.8335e−15	1.3512e−10	3.3280e−11	2.0040e−10	3.4728e−10	1.8236e−15
800×800	2.2264e−15	4.1668e−10	1.0388e−10	9.8822e−10	7.6756e−10	2.8183e−15
1600×1600	3.6671e−15	5.6204e−09	5.9614e−10	2.0064e−09	4.8494e−09	3.1498e−15

Table 3: Orszag−Tang benchmark. Conservation properties of the FV-FEEC scheme. "Error" (5.3) of the MHD conserved variables at different mesh resolutions.

In Figure 10, we report the L^1-error of the primitive MHD variables at final time $T = 1$ computed with respect to the second order reference solution. The observed convergence rate is around 0.6.

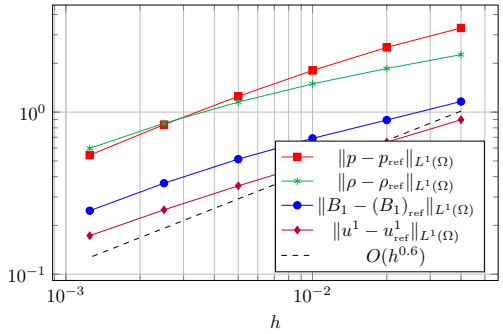

Figure 10: Orszag−Tang benchmark. Plot of the L^1-error vs. the mesh width h. The error of the MHD primitive variables is computed at final time $t = 1$ and with respect to a reference solution on a 3200×3200 mesh.

Finally, the ability of the FV-FEEC scheme to reproduce physically reliable solutions with rather sharp resolution of the shock fronts is gauged in Figure 11, see also the results available in literature e.g. [21, Section 3.4] or [62, Section 6.4]. The lowest order FV-FEEC is admittedly diffusive and does not capture all the complex shock interaction features visible in the second order accurate solution in Figure 11 (right column). Neither the FV-FEEC nor the second order reference solution manage to reproduce the current sheet characterizing the center of the domain in the second component of the $\mathbf{B}$ field.

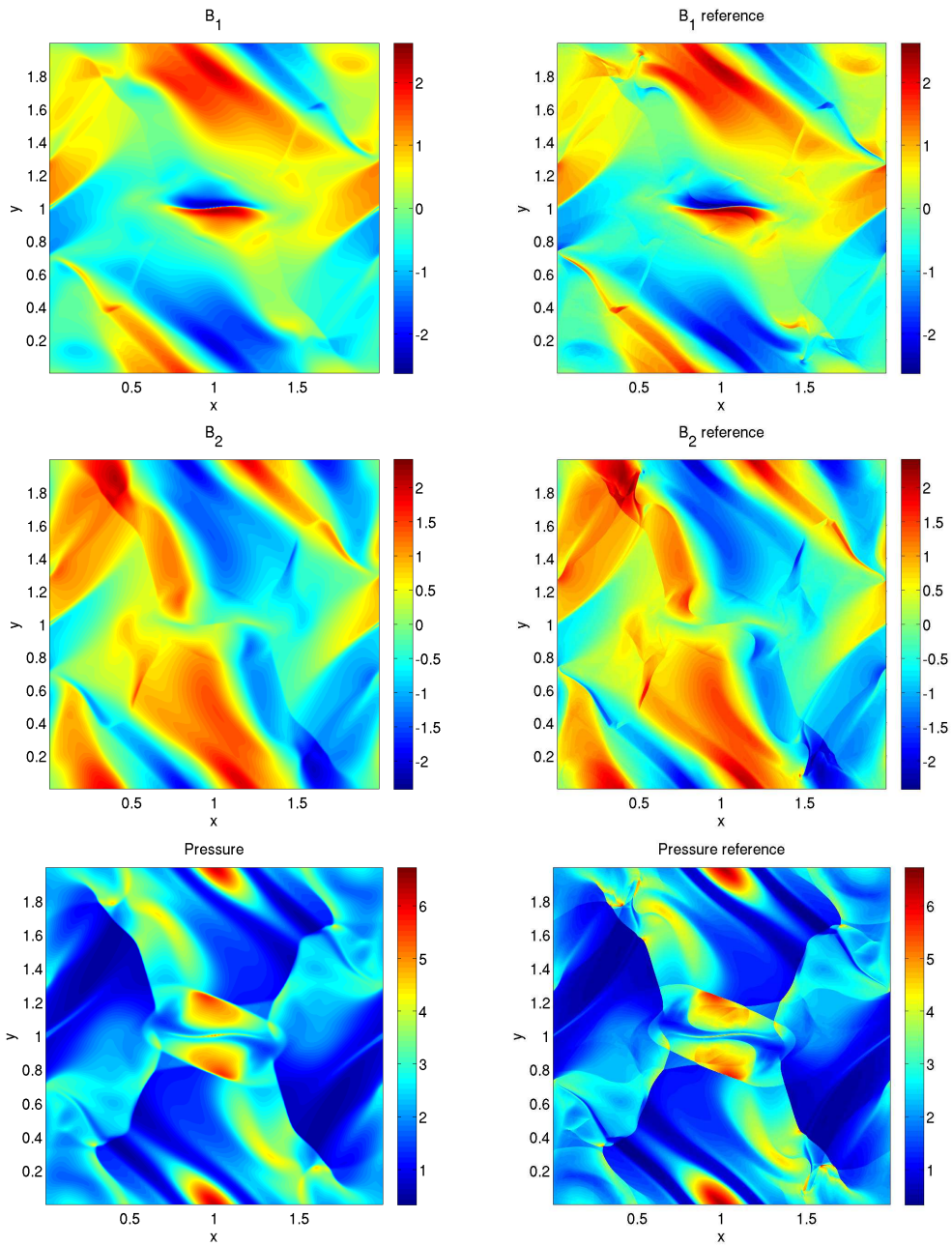

Figure 11: Orszag−Tang benchmark. On the left, numerical solution on a 1600×1600 Cartesian mesh obtained with the FV-FEEC scheme and Heun timestepping with $C_{\mathsf{CFL}} = 0.4$. Finite volume scheme for the extended Euler equations based on the HLL approximate Riemann solver. The color map is scaled to the extrema of the reference solution on a 3200×3200 mesh (right column).

5.3.4 Rotor Problem

A key dimensionless parameter for ideal MHD models is the so-called *plasma beta*, the ratio of thermal to magnetic pressure, $\beta = 2\mu_0 p / \|\mathbf{B}\|^2_{L^2}$, where μ_0 is the permeability of free space. Delivering physically admissible solutions in presence of low-beta plasmas ($\beta \ll 1$) is particularly challenging for numerical schemes. The rotor problem provides a numerical test for the low-beta plasma setting. It was introduced in [8, Section 3.1] to test the emergence and propagation of torsional Alfvén waves. The interior of the rotor is characterized by low values of the pressure, so that the test is also well-suited to attest the robustness of a numerical method in preserving positivity. The initial set up consists of a dense spinning

cylinder (the rotor) of radius 0.05, surrounded by the ambient fluid at rest which occupies the remaining part of the computational domain $\Omega = [0,1]^2$. The initial magnetic field is uniform but, as the rotor spins with the initial rotating velocity, the magnetic field in the x-direction starts wrapping around the rotor causing torsional Alfvén waves to propagate into the ambient fluid. As a result, the angular momentum will eventually decrease while the rotor will experience compression under the effect of the increased magnetic pressure assuming an oblong shape.

The physical problem is set up on an unbounded domain. This translates into artificial non-reflecting Neumann-type boundary conditions for the conserved variables entering the extended Euler system. Concerning the magnetic advection problem, the evolution of the velocity field guarantees that no inflow boundaries will occur at any time. The initial data are as explained above and characterized by,

$$\rho_0(x,y) = \begin{cases} 10 & \text{if } r < 0.1, \\ 1+9f & \text{if } 0.1 < r < 0.115, \\ 1 & \text{if } r > 0.115, \end{cases}$$

$$p_0(x,y) = 0.5,$$

$$u_0^1(x,y) = \begin{cases} 5-10y & \text{if } r < 0.1, \\ (5-10y)f & \text{if } 0.1 < r < 0.115, \\ 0 & \text{if } r > 0.115, \end{cases} \qquad u_0^2(x,y) = \begin{cases} 10x-5 & \text{if } r < 0.1, \\ (10x-5)f & \text{if } 0.1 < r < 0.115, \\ 0 & \text{if } r > 0.115, \end{cases}$$

$$\mathbf{B}_0(x,y) = \left(\frac{2.5}{\sqrt{4\pi}}, 0\right)^\top, \quad A_0(x,y) = \frac{2.5}{\sqrt{4\pi}} y,$$

where $r := \sqrt{(x-0.5)^2 + (y-0.5)^2}$, $f := (23 - 200r)/3$ and the gas constant is $\gamma = 5/3$. The simulation runs until time $T = 0.295$.

In order to numerically analyze the conservative properties of the FV-FEEC scheme tested on the rotor problem, Table 4 reports the error (5.3) on the conserved variables.

$\sharp\mathcal{T}_h$	$\mathcal{E}_r(\rho)$	$\mathcal{E}(\rho u^1)$	$\mathcal{E}(\rho u^2)$	$\mathcal{E}_r(B_1)$	$\mathcal{E}(B_2)$	$\mathcal{E}_r(E)$
200×200	4.3462e−04	4.1243e−11	2.3873e−12	4.8734e−04	3.0872e−04	9.3236e−04
400×400	8.2870e−05	9.7000e−12	4.3911e−11	9.9092e−05	6.5086e−08	1.7748e−04
800×800	5.5013e−06	3.5593e−11	4.5438e−10	6.7642e−06	1.1632e−10	1.1712e−05
1600×1600	1.0410e−07	1.6785e−08	5.7213e−07	1.3463e−07	1.7050e−09	2.2139e−07

Table 4: Rotor problem. Conservation properties of the FV-FEEC scheme. "Error" (5.3) of the MHD conserved variables at different mesh resolutions.

The FV-FEEC performs robustly also in the rotor test, as attested by Figure 12. The scheme captures many of the features of the MHD rotor flow being however rather diffusive when compared with the second order reference solution.

5.3.5 Blast Wave Problem

As a last test case, we consider the isothermal blast wave problem proposed in [5, Section 6.2.2]. Note that we did not develop a numerical scheme tailored to the isothermal MHD model, we rather "emulated" the isothermal behavior by setting the ratio of specific heats close to unitary ($\gamma = 1.001$ in the forthcoming simulations). The blast wave benchmark is numerically challenging because it is characterized by a highly anisotropic explosion spreading out from a high density cloud initialized in a circular region of the domain. As pointed out in [5], failing to provide a control of the divergence of the induction field can

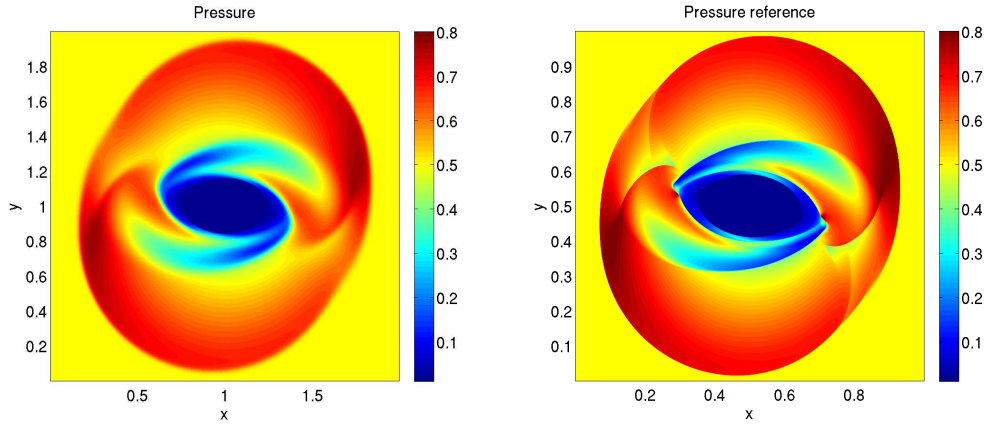

Figure 12: Rotor problem. Numerical solution on a 1600×1600 Cartesian mesh obtained with the lowest order FV-FEEC scheme and Heun timestepping with $C_{\mathsf{CFL}} = 0.4$. Finite volume scheme for the extended Euler equations based on the HLL approximate Riemann solver. The color map of the pressure plot is scaled to the extrema of the reference solution on a 3200×3200 mesh, shown on the top right plot.

engender detrimental small-scale fluctuations. In the domain $\Omega = [0,1]^2$ the initial data are,

$$\rho_0(x,y) = p_0(x,y) = \begin{cases} 100 & \text{if } \sqrt{(x-0.5)^2 + (y-0.5)^2} < 0.05, \\ 1 & \text{otherwise,} \end{cases}$$

$$\mathbf{u}_0(x,y) = \mathbf{0},$$

$$\mathbf{B}_0(x,y) = \left(\frac{5}{\sqrt{\pi}}, 0\right)^\top, \quad A_0(x,y) = \frac{5}{\sqrt{\pi}} y.$$

The simulation spans the time interval $I = [0, 0.09]$. Boundary conditions are of non-reflecting Neumann-type for the extended Euler variables, and the velocity field gives no inflow boundary.

The conservative properties of the scheme are numerically gauged in Table 5 where the error defined in (5.3) on the conserved variables is reported.

$\sharp\mathcal{T}_h$	$\mathcal{E}_r(\rho)$	$\mathcal{E}(\rho u^1)$	$\mathcal{E}(\rho u^2)$	$\mathcal{E}_r(B_1)$	$\mathcal{E}(B_2)$	$\mathcal{E}_r(E)$
200×200	8.5943e−14	1.3769e−12	5.8536e−11	7.8382e−15	4.3338e−11	8.9687e−14
400×400	2.6538e−15	8.6998e−12	7.5751e−10	1.7876e−15	1.7969e−10	3.9629e−15
800×800	2.0471e−15	1.8790e−11	1.4140e−09	2.8231e−15	1.1313e−10	9.6211e−15
1600×1600	2.1693e−14	7.6349e−08	6.4150e−07	9.9568e−14	5.3582e−09	1.8401e−14

Table 5: Blast wave test. Conservation properties of the FV-FEEC scheme. "Error" (5.3) of the MHD conserved variables at different mesh resolutions.

Numerical instabilities are a typical outcome of the blast wave test even for lowest order finite volume approximations of the full MHD system, see [21, pp. 356-357]. The blast wave MHD flow is characterized by outward- and inward-going fast magnetosonic shock and the magnetic induction field experiences a strong compression on account of the explosion. As it can be observed in Figure 13, the FV-FEEC scheme is robust, oscillations-free and it approximates the shocks rather sharply. The second row of Figure 13 shows the magnetic induction field lines: no fluctuations are observed, not even in the middle of the computational domain (compare with [5, Figure 9] and [21, Figure 8]).

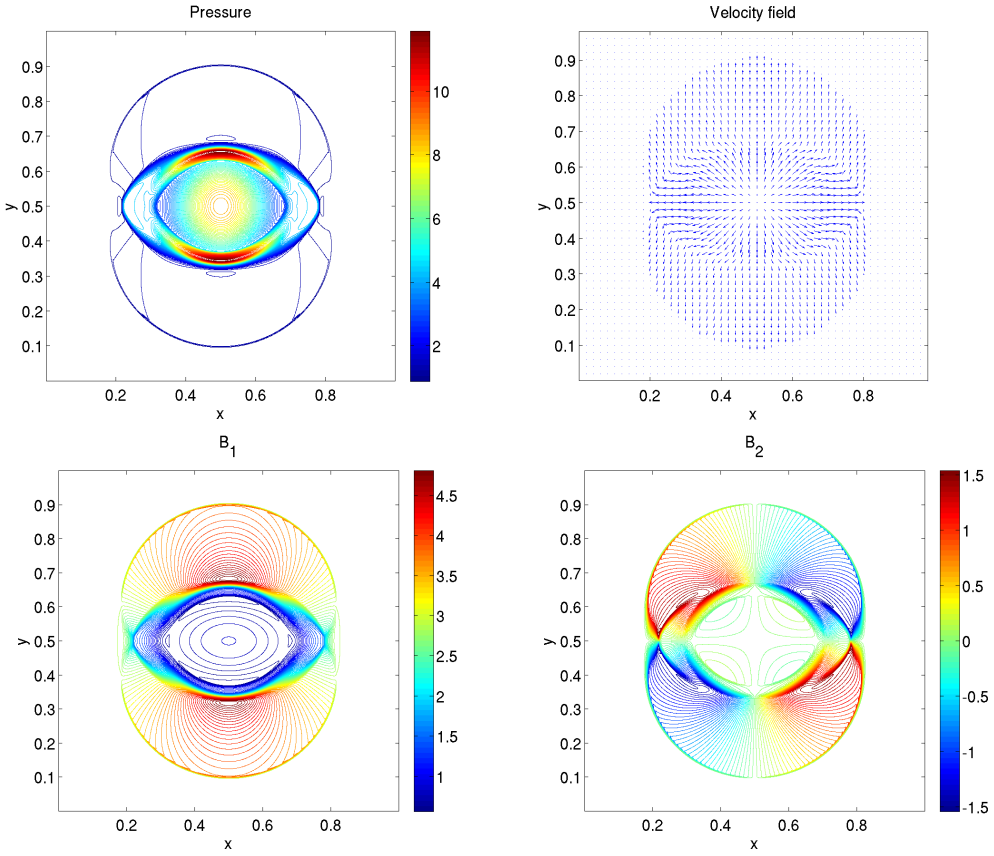

Figure 13: Blast wave test. Numerical discretization on a 1600×1600 Cartesian mesh with lowest order FV-FEEC scheme and Heun timestepping, $C_{\mathsf{CFL}} = 0.4$. Finite volume scheme for the extended Euler equations using HLL approximate Riemann solver.

6 Concluding Remarks

We have developed a family of numerical methods to solve the single-fluid standard MHD problem by coupling two different spatial discretizations of fluid and electromagnetic variables. The evolution of the electromagnetic fields relies on FEEC-based finite element approximations which ensure that the divergence constraint is satisfied exactly, and no mesh-staggering of fluid and electromagnetic variables, typical of constrained transport and "central schemes" for hyperbolic problems, is required. The extrusion contraction upwind schemes for the generalized advection problem are characterized by an intrinsic upwinding, which acts as a linear stabilization in the presence of boundary and internal layers. Moreover, the resulting discrete Lie derivative commutes with the exterior derivative which implies that closed discrete forms are Lie advected into closed forms, and hence both a potential-based and a **B**-based formulations can be used without compromising the divergence constraint. Although supported by numerical evidence, a rigorous stability and convergence analysis of the extrusion contraction upwind schemes is still an open problem.

Concerning the fluid dynamics part of the MHD model, we treated the balance equations for the fluid as a system of conservation laws with a varying coefficient, the magnetic induction field. Finite volume schemes have been used for the numerical discretizations of the extended Euler equations and they hinge on approximate Riemann solvers tailored to accommodate the presence of the magnetic induction as in [22]. The further adaptation of this construction to design numerical fluxes yielding a discrete version of the entropy inequality would pave the way to entropy stable schemes of arbitrarily high order.

Coupling the FEEC-based methods for the magnetic advection with the finite volume schemes for the fluid results in numerical methods for the ideal MHD system. The lowest order FV-FEEC schemes are first order accurate for smooth solutions, possess built-in structure preserving properties, and perform

robustly in many challenging MHD benchmark tests. The promising numerical results obtained when using discretizations of the electromagnetic fields based on discrete differential forms, even in the presence of complex flows, suggest that structure preserving conforming discretizations can be competitive also in computational fluid dynamics, typically preserve of finite volume and discontinuous Galerkin methods. Analogous splitting-based numerical methods for the MHD system obtained via fully discontinuous Galerkin discretizations of the potential-based advection problem (by staggering the magnetic potential with respect to the fluid variables similarly to a Yee-type scheme [63]) yield unphysical solutions on some challenging benchmark tests, as documented in [52, Section 7.2].

Beyond ideal MHD, extending the FV-FEEC approach to resistive MHD (1.1) is straightforward: We need only augment the discrete magnetic transport equation with a conventional conforming Galerkin discretization of the diffusion operator. As easy is the seamless coupling of the resistive MHD model (1.1) with a standard eddy current model in order to cover situations as outlined in Figure 14. If the plasma is confined to a bounded region in space, zero outflow conditions can be imposed for the fluid model at its boundary, whereas the FEEC discretization of the **A**-based formulation of the magneto-quasistatic equations can be used everywhere. It will ensure tangential continuity of both the magnetic vector potential and of the magnetic field (in a weak sense) across the plasma boundary.

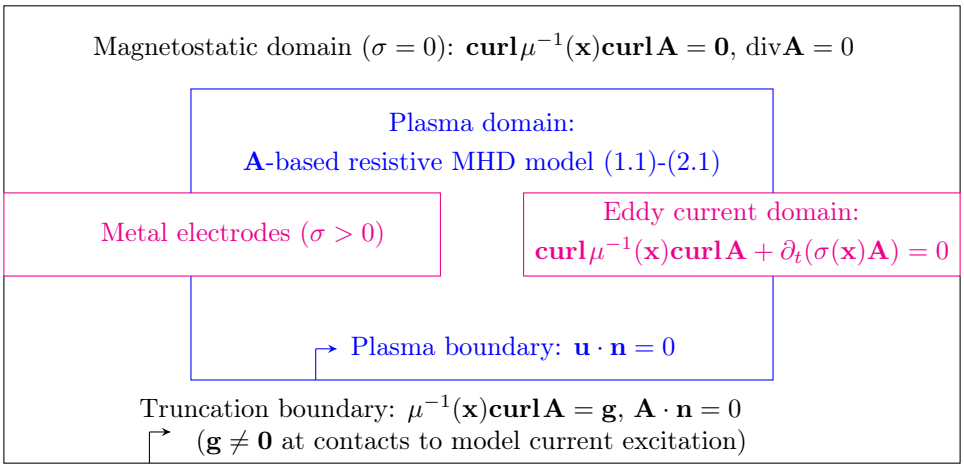

Figure 14: High-current circuit breaker set-up: resistive MHD inside an air chamber has to be coupled with an eddy current model outside. The symmetric positive semi-definite tensors $\sigma = \sigma(\mathbf{x})$ and $\mu = \mu(\mathbf{x})$ represent the spatially varying fluid electric conductivity and magnetic permeability, respectively.

6.1 Towards Higher Order FV-FEEC Schemes

The promising numerical results obtained with the lowest order FV-FEEC discretizations can be a starting point for the design of second and higher order accurate schemes. The "synchronization" of the coupling step in Algorithm 1 ensures that no additional error associated with the splitting is introduced. We can therefore identify two main components in the derivation of formally high order FV-FEEC schemes:

1. A high order discretization of the transient advection problem, able to supply a magnetic induction field accurate to the same order and endowed with a nonlinear mechanism for damping oscillations, capable of ensuring some TVD-like property without affecting the accuracy of the scheme;

2. A high order extension of the finite volume schemes for the extended Euler equations via reconstruction and limiting, with controls on the preservation and evolution of physically admissible states.

Concerning the first aspect, when resorting to the potential-based formulation of the advection problem, high order numerical schemes should ideally curb the emergence of spurious oscillations in both the

magnetic potential and the magnetic induction field. Except for the constrained transport method with TVD slope limiters based on "wave differences" developed in [56], numerical strategies to tackle Gibbs phenomena in some derivative of the solution have rarely been considered. In the context of extrusion contraction upwind schemes, *entropy viscosity methods* [28, 29] seem particularly attractive for the aforementioned task since they are based on the addition of a degenerate nonlinear diffusion term tuned locally by a numerical viscosity proportional to the local entropy production. Specifically, the commutativity of the exterior derivative and the discrete Lie derivative allows the construction of nonlinear residual-based viscosity schemes for the advection of the magnetic potential, based, however, on the (entropy) residual of the magnetic induction equation. Preliminary results in this direction can be found in [52, Section 4.4]. In the alternative situation occurring when directly discretizing the magnetic induction problem, one should rely on the addition of artificial magnetic diffusion, based again on the induction residual. The augmented discrete operator obtained from the Lie derivative plus the second order artificial diffusion will still satisfy a commuting diagram property. On the other hand, it is not straightforward to gauge the effectiveness of the artificial viscosity since the nonlinear second order stabilization will have no impact on the kernel of the exterior derivative.

High order finite volume schemes for the extended Euler equations can be designed via ENO and WENO reconstruction techniques [31, 59]. The resulting schemes prove numerically robust and provide non-oscillatory solutions [52, Section 6.3.2], but they are not provably positively conservative. Devising a positivity fix for the finite volume discretizations of the extended Euler system in order to guarantee admissible updated and evolved fluid variables seems a challenging task since the lowest order scheme itself is not provably positively conservative. These issues represent intriguing topics for further investigation.

Acknowledgment. The authors thank Siddhartha Mishra for many fruitful discussions and helpful comments. This work was partially supported by Swiss NSF Grant No. 146355.

A Magnetic Advection-Diffusion for the Magnetic Potential

The magneto-quasistatic Maxwell's equations (eddy current model) for conductors moving with velocity $\mathbf{u}$ reads

$$\begin{aligned} \mathbf{curl}\,\mathbf{E} + \partial_t \mathbf{B} = 0, &\quad \text{(Faraday's law)} & \mathbf{B} = \mu \mathbf{H}, &\quad \text{(material law)} \\ \mathbf{curl}\,\mathbf{H} = \mathbf{J}, &\quad \text{(Ampère's law)} & \mathbf{J} = \sigma(\mathbf{E} + \mathbf{u} \times \mathbf{B}), &\quad \text{(Ohm's law)} \\ \mathrm{div}\mathbf{B} = 0, &\quad \text{(Gauss' law)} \end{aligned}$$

where $\mathbf{E}$ is the electric field, $\mathbf{H}$ the magnetic field and $\mathbf{J}$ the electric current, $\sigma = \sigma(\mathbf{x})$ is the electric conductivity and $\mu = \mu(\mathbf{x})$ the magnetic permeability.

By considering the electric field in the moving frame $\widetilde{\mathbf{E}} := \mathbf{E} + \mathbf{u} \times \mathbf{B}$, one can write $\mathbf{curl}\,\mathbf{H} = \sigma \widetilde{\mathbf{E}}$ and $\mathbf{curl}\,\widetilde{\mathbf{E}} = -(\partial_t \mathbf{B} + \mathbf{curl}\,(\mathbf{B} \times \mathbf{u}) + \mathbf{u}\mathrm{div}\mathbf{B})$ yielding the magnetic induction equation (1.1d)

$$\mathbf{curl}\,\sigma^{-1}\mathbf{curl}\,\mathbf{H} + \partial_t \mathbf{B} + \mathbf{curl}\,(\mathbf{B} \times \mathbf{u}) + \mathbf{u}\mathrm{div}\mathbf{B} = \mathbf{0}.$$

Alternatively, the eddy current model can be equivalently reformulated in terms of the magnetic vector potential ($\mathbf{A}$-based formulation). The constraint $\mathrm{div}\mathbf{B} = 0$ implies that the magnetic induction field $\mathbf{B}$ can be written as $\mathbf{B} = \mathbf{curl}\,\mathbf{A}$. Using again the electric field $\widetilde{\mathbf{E}}$,

$$\mathbf{curl}\,\widetilde{\mathbf{E}} = -(\partial_t \mathbf{B} + \mathbf{curl}\,(\mathbf{B} \times \mathbf{u})) = \mathbf{curl}\,(-\partial_t \mathbf{A} - \mathbf{curl}\,\mathbf{A} \times \mathbf{u}) - \mathbf{curl}\,(\mathrm{grad}(\mathbf{u} \cdot \mathbf{A})),$$

where the last term evaluates to zero. Therefore, $\widetilde{\mathbf{E}} = -\partial_t \mathbf{A} - \mathbf{curl}\,\mathbf{A} \times \mathbf{u} - \mathrm{grad}(\mathbf{u} \cdot \mathbf{A}) - \mathrm{grad}\varphi$, where φ is a scalar potential. Thanks to gauge freedom we may opt for the Weyl or temporal gauge and set $\varphi = 0$. Then, using the material law $\mathbf{H} = \mu^{-1}\mathbf{B} = \mu^{-1}\mathbf{curl}\,\mathbf{A}$ we arrive at the transient advection-diffusion equation (2.1) for the magnetic potential,

$$\mathbf{curl}\,(\mu^{-1}\mathbf{curl}\,\mathbf{A}) + \sigma(\partial_t \mathbf{A} + \mathbf{curl}\,\mathbf{A} \times \mathbf{u} + \mathrm{grad}(\mathbf{u} \cdot \mathbf{A})) = \mathbf{0}.$$

The parameters $\sigma(\mathbf{x})$ and $\mu(\mathbf{x})$ are assumed to be spatially varying positive semi-definite tensors. Moreover, suitable initial and boundary conditions have to imposed. We refer to [52, Section 2.2] for an analogous manipulation of the eddy current model in the framework of exterior calculus.

References

[1] D. N. Arnold and G. Awanou. "The serendipity family of finite elements." In: *Found. Comput. Math.* 11.3 (2011), pp. 337–344. URL: http://dx.doi.org/10.1007/s10208-011-9087-3.

[2] D. N. Arnold, D. Boffi, and F. Bonizzoni. "Finite element differential forms on curvilinear cubic meshes and their approximation properties." In: *Numer. Math.* 129.1 (2015), pp. 1–20. URL: http://dx.doi.org/10.1007/s00211-014-0631-3.

[3] D. N. Arnold, F. Brezzi, B. Cockburn, and L. D. Marini. "Unified analysis of discontinuous Galerkin methods for elliptic problems." In: *SIAM J. Numer. Anal.* 39.5 (2001/02), pp. 1749–1779. URL: http://dx.doi.org/10.1137/S0036142901384162.

[4] D. N. Arnold, R. S. Falk, and R. Winther. "Finite element exterior calculus, homological techniques, and applications." In: *Acta Numer.* 15 (2006), pp. 1–155. URL: http://dx.doi.org/10.1017/S0962492906210018.

[5] D. S. Balsara. "Total variation diminishing scheme for adiabatic and isothermal magnetohydrodynamics." In: *The Astrophysical Journal Supplement Series* 116.1 (1998), p. 133. URL: http://stacks.iop.org/0067-0049/116/i=1/a=133.

[6] D. S. Balsara. "Divergence-free adaptive mesh refinement for magnetohydrodynamics." In: *J. Comput. Phys.* 174.2 (Dec. 2001), pp. 614–648. URL: http://dx.doi.org/10.1006/jcph.2001.6917.

[7] D. S. Balsara. "Second-order-accurate schemes for magnetohydrodynamics with divergence-free reconstruction." In: *The Astrophysical Journal Supplement Series* 151.1 (2004), p. 149. URL: http://stacks.iop.org/0067-0049/151/i=1/a=149.

[8] D. S. Balsara and D. S. Spicer. "A staggered mesh algorithm using high order Godunov fluxes to ensure solenoidal magnetic fields in magnetohydrodynamic simulations." In: *J. Comput. Phys.* 149.2 (1999), pp. 270–292. URL: http://dx.doi.org/10.1006/jcph.1998.6153.

[9] A. Bossavit. "Extrusion, contraction: their discretization via Whitney forms." In: *COMPEL* 22.3 (2003), pp. 470–480. URL: http://dx.doi.org/10.1108/03321640310474877.

[10] F. Bouchut, C. Klingenberg, and K. Waagan. "A multiwave approximate Riemann solver for ideal MHD based on relaxation. I. Theoretical framework." In: *Numer. Math.* 108.1 (2007), pp. 7–42. URL: http://dx.doi.org/10.1007/s00211-007-0108-8.

[11] J. U. Brackbill and D. C. Barnes. "The effect of nonzero $\nabla \cdot \mathbf{B}$ on the numerical solution of the magnetohydrodynamic equations." In: *J. Comput. Phys.* 35.3 (1980), pp. 426–430. URL: http://dx.doi.org/10.1016/0021-9991(80)90079-0.

[12] M. Brio and C.-C. Wu. "An upwind differencing scheme for the equations of ideal magnetohydrodynamics." In: *J. Comput. Phys.* 75.2 (1988), pp. 400–422. URL: http://dx.doi.org/10.1016/0021-9991(88)90120-9.

[13] P. Cargo and G. Gallice. "Roe matrices for ideal MHD and systematic construction of Roe matrices for systems of conservation laws." In: *J. Comput. Phys.* 136.2 (1997), pp. 446–466. URL: http://dx.doi.org/10.1006/jcph.1997.5773.

[14] P. G. Ciarlet. *The finite element method for elliptic problems*. North-Holland Publishing Co., Amsterdam-New York-Oxford, 1978, pp. xix+530.

[15] B. Cockburn and C.-W. Shu. "The Runge-Kutta discontinuous Galerkin method for conservation laws. V. Multidimensional systems." In: *J. Comput. Phys.* 141.2 (1998), pp. 199–224. URL: http://dx.doi.org/10.1006/jcph.1998.5892.

[16] A. Dedner, F. Kemm, D. Kröner, C.-D. Munz, T. Schnitzer, and M. Wesenberg. "Hyperbolic divergence cleaning for the MHD equations." In: *J. Comput. Phys.* 175.2 (2002), pp. 645–673. URL: http://dx.doi.org/10.1006/jcph.2001.6961.

[17] M. Desbrun, A. N. Hirani, M. Leok, and J. E. Marsden. *Discrete exterior calculus*. 2005. URL: https://arxiv.org/abs/math/0508341v2.

[18] B. Einfeldt. "On Godunov-type methods for gas dynamics." In: *SIAM J. Numer. Anal.* 25.2 (1988), pp. 294–318. URL: http://dx.doi.org/10.1137/0725021.

[19] B. Einfeldt, C.-D. Munz, P. L. Roe, and B. Sjögreen. "On Godunov-type methods near low densities." In: *J. Comput. Phys.* 92.2 (1991), pp. 273–295. URL: http://dx.doi.org/10.1016/0021-9991(91)90211-3.

[20] F. G. Fuchs, K. H. Karlsen, S. Mishra, and N. H. Risebro. "Stable upwind schemes for the magnetic induction equation." In: *M2AN Math. Model. Numer. Anal.* 43.5 (2009), pp. 825–852. URL: http://dx.doi.org/10.1051/m2an/2009006.

[21] F. G. Fuchs, A. D. McMurry, S. Mishra, N. H. Risebro, and K. Waagan. "Approximate Riemann solvers and robust high-order finite volume schemes for multi-dimensional ideal MHD equations." In: *Commun. Comput. Phys.* 9.2 (2011), pp. 324–362. URL: http://dx.doi.org/10.4208/cicp.171109.070510a.

[22] F. G. Fuchs, S. Mishra, and N. H. Risebro. "Splitting based finite volume schemes for ideal MHD equations." In: *J. Comput. Phys.* 228.3 (2009), pp. 641–660. URL: http://dx.doi.org/10.1016/j.jcp.2008.09.027.

[23] J. Glimm. "Solutions in the large for nonlinear hyperbolic systems of equations." In: *Comm. Pure Appl. Math.* 18 (1965), pp. 697–715. URL: http://dx.doi.org/10.1002/cpa.3160180408.

[24] E. Godlewski and P.-A. Raviart. *Numerical approximation of hyperbolic systems of conservation laws*. Vol. 118. Applied Mathematical Sciences. Springer-Verlag, New York, 1996, pp. viii+509. URL: http://dx.doi.org/10.1007/978-1-4612-0713-9.

[25] H. Goedbloed and S. Poedts. *Principles of Magnetohydrodynamics*. Cambridge University Press, 2004.

[26] D. Gottlieb and J. S. Hesthaven. "Spectral methods for hyperbolic problems." In: *J. Comput. Appl. Math.* 128.1-2 (2001), pp. 83–131. URL: http://dx.doi.org/10.1016/S0377-0427(00)00510-0.

[27] S. Gottlieb, C.-W. Shu, and E. Tadmor. "Strong stability-preserving high-order time discretization methods." In: *SIAM Rev.* 43.1 (2001), 89–112 (electronic). URL: http://dx.doi.org/10.1137/S003614450036757X.

[28] J.-L. Guermond and R. Pasquetti. "Entropy-based nonlinear viscosity for Fourier approximations of conservation laws." In: *C. R. Math. Acad. Sci. Paris* 346.13-14 (2008), pp. 801–806. URL: http://dx.doi.org/10.1016/j.crma.2008.05.013.

[29] J.-L. Guermond, R. Pasquetti, and B. Popov. "Entropy viscosity method for nonlinear conservation laws." In: *J. Comput. Phys.* 230.11 (2011), pp. 4248–4267. URL: http://dx.doi.org/10.1016/j.jcp.2010.11.043.

[30] K. F. Gurski. "An HLLC-type approximate Riemann solver for ideal magnetohydrodynamics." In: *SIAM J. Sci. Comput.* 25.6 (2004), 2165–2187 (electronic). URL: http://dx.doi.org/10.1137/S1064827502407962.

[31] A. Harten, B. Engquist, S. Osher, and S. R. Chakravarthy. "Uniformly high-order accurate essentially nonoscillatory schemes. III." In: *J. Comput. Phys.* 71.2 (1987), pp. 231–303. URL: http://dx.doi.org/10.1016/0021-9991(87)90031-3.

[32] A. Harten, P. D. Lax, and B. van Leer. "On upstream differencing and Godunov-type schemes for hyperbolic conservation laws." In: *SIAM Rev.* 25.1 (1983), pp. 35–61. URL: http://dx.doi.org/10.1137/1025002.

[33] J. F. Hawley and C. R. Evans. "Constraint preserving transport for magnetohydrodynamics." In: *Frontiers in numerical relativity (Urbana-Champaign, IL, 1988)*. Cambridge Univ. Press, Cambridge, 1989, pp. 179–193.

[34] H. Heumann and R. Hiptmair. *Extrusion contraction upwind schemes for convection-diffusion problems*. Tech. rep. 2008-30. Switzerland: Seminar for Applied Mathematics, ETH Zürich, 2008. URL: https://www.sam.math.ethz.ch/sam_reports/reports_final/reports2008/2008-30.pdf.

[35] H. Heumann and R. Hiptmair. "Eulerian and semi-Lagrangian methods for convection-diffusion for differential forms." In: *Discrete Contin. Dyn. Syst.* 29.4 (2011), pp. 1471–1495. URL: http://aimsciences.org/journals/displayArticlesnew.jsp?paperID=5720.

[36] H. Heumann, R. Hiptmair, and C. Pagliantini. "Stabilized Galerkin for transient advection of differential forms." In: *Discrete Contin. Dyn. Syst. Ser. S* 9.1 (2016), pp. 185–214. URL: http://dx.doi.org/10.3934/dcdss.2016.9.185.

[37] R. Hiptmair. "Canonical construction of finite elements." In: *Math. Comp.* 68.228 (1999), pp. 1325–1346. URL: http://dx.doi.org/10.1090/S0025-5718-99-01166-7.

[38] R. Hiptmair. "Finite elements in computational electromagnetism." In: *Acta Numer.* 11 (2002), pp. 237–339. URL: http://dx.doi.org/10.1017/S0962492902000041.

[39] K. Hu, Y. Ma, and J. Xu. "Stable finite element methods preserving $\nabla \cdot \mathbf{B} = 0$ exactly for MHD models." In: *Numerische Mathematik* (2016), pp. 1–26. URL: http://dx.doi.org/10.1007/s00211-016-0803-4.

[40] T. J. R. Hughes and A. Brooks. "A multidimensional upwind scheme with no crosswind diffusion." In: *Finite element methods for convection dominated flows*. Vol. 34. AMD. Amer. Soc. Mech. Engrs. (ASME), New York, 1979, pp. 19–35.

[41] T. J. R. Hughes, L. P. Franca, and G. M. Hulbert. "A new finite element formulation for computational fluid dynamics. VIII. The Galerkin/least-squares method for advective-diffusive equations." In: *Comput. Methods Appl. Mech. Engrg.* 73.2 (1989), pp. 173–189. URL: http://dx.doi.org/10.1016/0045-7825(89)90111-4.

[42] J. M. Hyman and M. Shashkov. "Mimetic discretizations for Maxwell's equations." In: *J. Comput. Phys.* 151.2 (1999), pp. 881–909. URL: http://dx.doi.org/10.1006/jcph.1999.6225.

[43] R. Käppeli, S. C. Whitehouse, S. Scheidegger, U.-L. Pen, and M. Liebendörfer. "FISH: a three-dimensional parallel magnetohydrodynamics code for astrophysical applications." In: *The Astrophysical Journal Supplement Series* 195.20 (2011), pp. 1–16. URL: http://stacks.iop.org/0067-0049/195/i=2/a=20.

[44] P. D. Lax. "Hyperbolic systems of conservation laws. II." In: *Comm. Pure Appl. Math.* 10 (1957), pp. 537–566. URL: http://dx.doi.org/10.1002/cpa.3160100406.

[45] R. J. LeVeque. *Finite volume methods for hyperbolic problems*. Cambridge Texts in Applied Mathematics. Cambridge University Press, Cambridge, 2002, pp. xx+558. URL: http://dx.doi.org/10.1017/CBO9780511791253.

[46] S. Li. "An HLLC Riemann solver for magneto-hydrodynamics." In: *J. Comput. Phys.* 203.1 (2005), pp. 344–357. URL: http://dx.doi.org/10.1016/j.jcp.2004.08.020.

[47] T. J. Linde. "A three-dimensional adaptive multifluid MHD model of the heliosphere." PhD thesis. The university of Michigan, Ann Arbor, MI, 1998.

[48] P. Londrillo and L. Del Zanna. "On the divergence-free condition in Godunov-type schemes for ideal magneto-hydrodynamics: the upwind constrained transport method." In: *J. Comput. Phys.* 195.1 (2004), pp. 17–48. URL: http://dx.doi.org/10.1016/j.jcp.2003.09.016.

[49] T. Miyoshi and K. Kusano. "A multi-state HLL approximate Riemann solver for ideal magnetohydrodynamics." In: *J. Comput. Phys.* 208.1 (2005), pp. 315–344. URL: http://dx.doi.org/10.1016/j.jcp.2005.02.017.

[50] P. Mullen, A. McKenzie, D. Pavlov, L. Durant, Y. Tong, E. Kanso, J. E. Marsden, and M. Desbrun. "Discrete Lie advection of differential forms." In: *Found. Comput. Math.* 11.2 (2011), pp. 131–149. URL: http://dx.doi.org/10.1007/s10208-010-9076-y.

[51] S. A. Orszag and C.-M. Tang. "Small-scale structure of two-dimensional magnetohydrodynamic turbulence." In: *J. Fluid Mech.* 90.1 (1979), pp. 129–143. URL: http://dx.doi.org/10.1017/S002211207900210X.

[52] C. Pagliantini. "Computational Magnetohydrodynamics with Discrete Differential Forms." PhD thesis. ETH Zürich, 2016. URL: http://dx.doi.org/10.3929/ethz-a-010722079.

[53] K. G. Powell. *An approximate Riemann solver for magnetohydrodynamics (that works in more than one dimension)*. Tech. rep. 94-24. Langley, VA, 1994.

[54] P.-A. Raviart and J.-M. Thomas. "A mixed finite element method for 2nd order elliptic problems." In: *Mathematical aspects of finite element methods (Proc. Conf., Consiglio Naz. delle Ricerche (C.N.R.), Rome, 1975)*. Springer, Berlin, 1977, 292–315. Lecture Notes in Math., Vol. 606.

[55] H.-G. Roos, M. Stynes, and L. Tobiska. *Robust numerical methods for singularly perturbed differential equations*. Second. Vol. 24. Springer Series in Computational Mathematics. Springer-Verlag, Berlin, 2008, pp. xiv+604.

[56] J. A. Rossmanith. "An unstaggered, high-resolution constrained transport method for magnetohydrodynamic flows." In: *SIAM J. Sci. Comput.* 28.5 (2006), pp. 1766–1797. URL: http://dx.doi.org/10.1137/050627022.

[57] D. Schötzau. "Mixed finite element methods for stationary incompressible magneto-hydrodynamics." In: *Numer. Math.* 96.4 (2004), pp. 771–800. URL: http://dx.doi.org/10.1007/s00211-003-0487-4.

[58] G. Schwarz. *Hodge decomposition − a method for solving boundary value problems*. Vol. 1607. Lecture Notes in Mathematics. Springer-Verlag, Berlin, 1995, pp. viii+155.

[59] C.-W. Shu and S. Osher. "Efficient implementation of essentially nonoscillatory shock-capturing schemes. II." In: *J. Comput. Phys.* 83.1 (1989), pp. 32–78. URL: http://dx.doi.org/10.1016/0021-9991(89)90222-2.

[60] M. Tabata. "A finite element approximation corresponding to the upwind finite differencing." In: *Mem. Numer. Math.* 4 (1977), pp. 47–63.

[61] E. F. Toro, M. Spruce, and W. Speares. "Restoration of the contact surface in the HLL-Riemann solver." In: *Shock Waves* 4.1 (1994), pp. 25–34. URL: http://dx.doi.org/10.1007/BF01414629.

[62] G. Tóth. "The $\nabla \cdot B = 0$ constraint in shock-capturing magnetohydrodynamics codes." In: *J. Comput. Phys.* 161.2 (2000), pp. 605–652. URL: http://dx.doi.org/10.1006/jcph.2000.6519.

[63] K. Yee. "Numerical solution of initial boundary value problems involving Maxwell's equations in isotropic media." In: *IEEE Transactions on Antennas and Propagation* 14.3 (1966), pp. 302–307. URL: https://doi.org/10.1109/TAP.1966.1138693.